# GEOMORPHOLOGICAL AND SEDIMENTOLOGICAL EVIDENCE OF LATE PLEISTOCENE GLACIATION IN THE BABIA GÓRA MASSIF (WESTERN FLYSCH CARPATHIANS, POLAND)

Piotr Kłapyta, Dawid Siemek

Institute of Geography and Spatial Management, Jagiellonian University, Kraków, Poland

Manuscript received: March 26, 2025
Revised version: May 27, 2025

Kłapyta P., Siemek D., 2026. Geomorphological and sedimentological evidence of Late Pleistocene glaciation in the Babia Góra massif (Western Flysch Carpathians, Poland). *Quaestiones Geographicae* 45(1), Bogucki Wydawnictwo Naukowe, Poznań, pp. 39–61. 9 figs, 2 tables.

**Abstract:** The legacy of Pleistocene glaciation in the Babia Góra massif (1725 m a.s.l.) has been the subject of vigorous debate for over a century. These controversies have been largely influenced by the poor preservation of glacial landforms and their extensive overprint by rock slope failures (RSFs). In this context, geomorphological criteria alone have proven insufficient for a comprehensive interpretation of glacial features in flysch lithology, which has been heavily shaped by landslides. In this study, we present the results of field and LiDAR-supported geomorphological mapping, clast morphology analysis and micromorphological examination of sand-sized quartz grains. This multi-proxy approach, when combined with previously published Schmidt-hammer data, provides robust evidence for the presence of glaciation in the Babia Góra massif. The Late Pleistocene palaeoglacier (area 0.87 km$^2$, 2.2 km long) was reconstructed in the headwaters of the Szumiąca Woda valley. Mapped latero-frontal moraines mark the extent of the glacier front at 930 m a.s.l. The glacier equilibrium line altitude (ELA) calculated from glacier hypsometry with the area altitude balance ratio (AABR) 1.6 was 1272 m. However, after accounting for the topographic effect of additional snow accumulation, the climatic ELA was recalculated and placed at 1354 m a.s.l. These findings suggest that, in addition to the previously known eastward horizontal gradient of ELA rise, a southward trend of rising ELA was also observed across the Western Carpathians.

**Keywords:** glacier reconstruction, clast morphology, SEM, Babia Góra, Western Carpathians

*Corresponding author: Piotr Kłapyta; piotr.klapyta@uj.edu.pl*

## Introduction

Glacial processes are effective geomorphological agents in shaping mountain relief regardless of hillslope topography, latitude and climate. The rate of glacial erosion is approximately an order of magnitude larger than that of fluvial erosion over time (Wilner et al. 2024); thus, pronounced glacial activity can significantly alter the original fluvial-erosional landscape. Glacier erosion particularly affects the areas located just below the glacier equilibrium line altitude (ELA), where glacial processes are the most effective (Pedersen, Egholm 2013). Glacial cirques form in the glacier accumulation zone (Evans 2006, 2021, Barr, Spagnolo 2015), whereas the longitudinal profiles of glaciated valleys are steepened in their upper sections and gradually flattened towards



https://doi.org/10.14746/quageo-2026-0003
ISSN 2082-2103, eISSN 2081-6383

the terminal moraines, which mark the glacial limit in the ablation zone (Anderson et al. 2012, Barr, Lovell 2014).

The bedrock lithology has a significant impact on glacier formation and cirque development (Evans 1977, Hughes et al. 2007, Mîndrescu, Evans 2014), as well as clast morphology and debris cascades in glaciated mountain environments (Lukas et al. 2013). The sedimentary flysch rocks (sandstones and mudstones) are considered relatively weak lithology, where glacial features are much poorly developed than in the crystalline and limestone lithology (Hughes et al. 2007, Mîndrescu, Evans 2014, Kłapyta et al. 2023a). The soft and highly anisotropic flysch clasts show potentially fast glacial abrasion and concomitant fracturing (Lukas et al. 2013).

In the Carpathians, glacial landscapes have been documented in 36 mountain massifs (Pawłowski 1936, Urdea et al. 2022, Kłapyta et al. 2023a) (Fig. 1A). In the Eastern Carpathians, most glaciers developed within flysch formations. The morphological similarity between mapped moraines and rock slope failures (RSFs) was already highlighted by geomorphologists studying in this area (Sawicki 1912, Pawłowski 1936, Świderski 1938, Sîrcu 1962, 1963, Wójcik 1994). As a result, glacier reconstruction based solely on the geomorphological record proved to be challenging. To address this, the term 'pseudoglacial

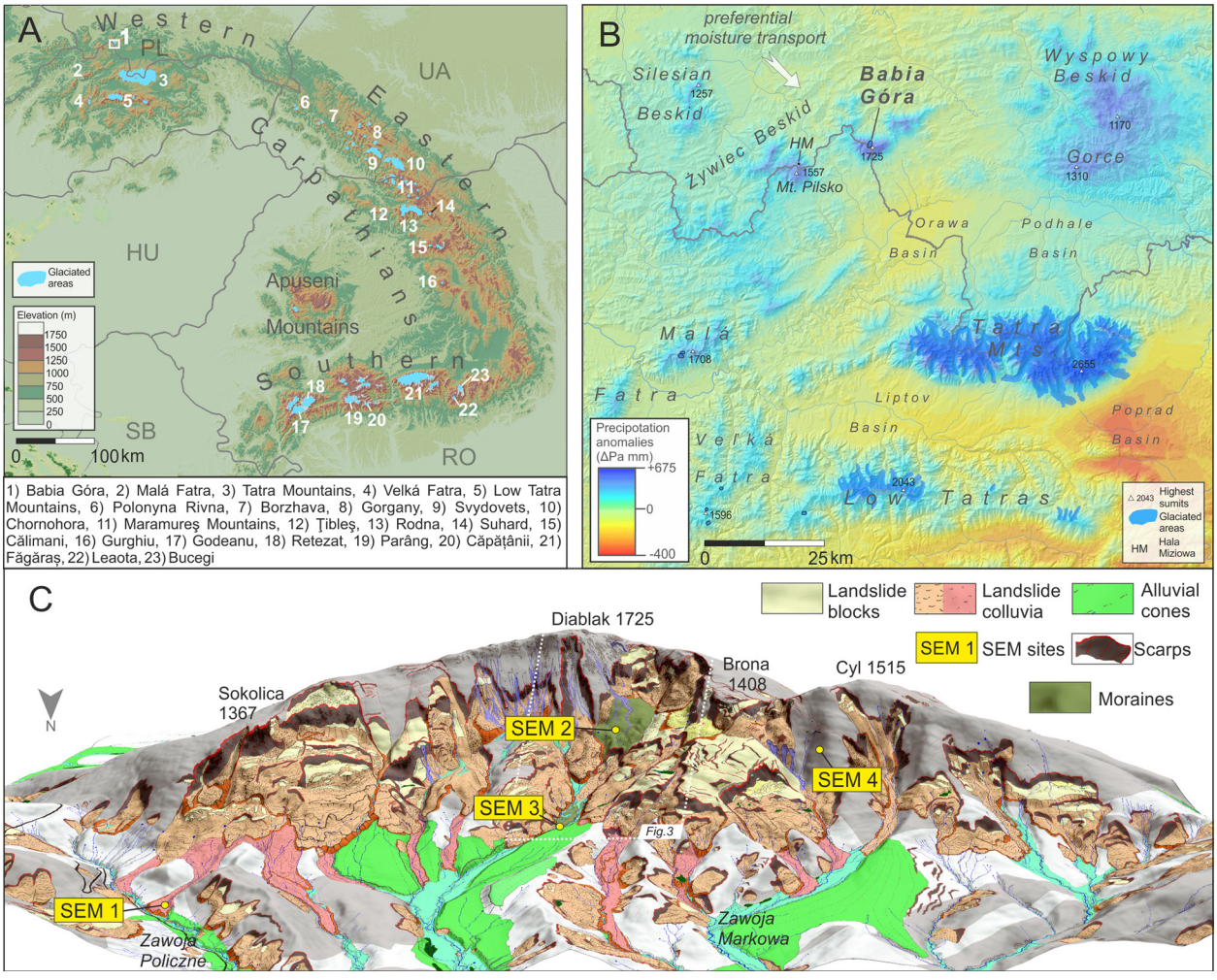


Fig. 1. Location of the study area within the regional context of the glaciated mountain massifs in the Carpathians, according to Kłapyta et al. (2023a, b). A – distribution of precipitation anomalies in relation to the mean (1970–2000) in the Western Carpathians based on the climate data (Worldclim 2.1 dataset; Fick, Hijmans 2017). The extent of glaciers according to Zasadni and Kłapyta (2014) and Pyrda (2025). B – general view of the morphology of the northern slope of Babia Góra. The geomorphological map (Kłapyta 2020) is projected onto the LiDAR-derived digital terrain model (DTM). C – yellow circles indicate the location of scanning electron microscopy (SEM) sampling sites.

morphology' was introduced in the Polish geomorphological literature (Sawicki 1913, Ziętara 1962) to describe atypical features that could be similar to glacial but formed by non-glacial processes, mainly RSFs. Despite these limitations, the use of sedimentological methods reveals notable differences in the roundness and sorting of gravel fractions between moraines and fluvioglacial deposits in the Chornohora (Miller 1963) and Svydovets massifs (Ananev 1981). Clast morphology analyses carried out in selected test areas in the Eastern Carpathians (Kłapyta et al. 2021b, 2022a, b) showed that the key determinant of moraine clast morphology in the flysch areas is the rounding index (RA), which allows for distinguishing moraines from slope and fluvial deposits. These findings are consistent with the debris cascade model in glaciated areas built with highly anisotropic rocks (known as type II catchments; Lukas et al. 2013), where the initial significant angularity of clasts is reduced through subglacial and fluvial transport with minor shape changes.

In the Western Carpathians, glacial landscapes have developed in the areas built mostly with igneous and metamorphic rocks (Lukniš 1964, Zasadni, Kłapyta 2014) of the Palaeozoic basement (Maglay et al. 2011) (Fig. 1). The Babia Góra massif is the only formerly glaciated area in the Western Carpathians built with flysch. The legacy of the Pleistocene glaciation in this area has been a contentious issue for over a century (Sawicki 1913, Ziętara, Ziętara 1958, Ziętara 1962, Kłapyta 2020, Łajczak 1981, 1998, 2023). These controversies were related to poor morphological preservation of glacial landforms and their extensive overprint by RSFs. Previous studies primarily relied on geomorphological evidence, which proved to be unreliable in areas with a high frequency of landslides, leading to inconsistencies in interpreting glacial features (Ziętara, Ziętara 1958, Ziętara 1962). The advent of LiDAR digital elevation models (DEMs) and results of detailed geomorphological mapping (Kłapyta 2020) have opened a new perspective for more robust interpretation of landforms in this area and detailed inventory of RSFs (Kłapyta et al. 2025). Additionally, application of Schmidt-hammer relative age dating allow to establish the evolutionary pattern of landslides on the northern slope of the Babia Góra (Kłapyta et al. 2025).

This study aims to present geomorphologic and sedimentological evidence of Pleistocene glaciation in the Babia Góra massif. In this study, we provide a multiproxy approach that combines LiDAR-based geomorphological mapping, sedimentological analysis and scanning electron microscopy (SEM) analysis of sand-size quartz grain micromorphology. Additionally, we reconstruct the glacier geometry and associated ELAs as well as discuss the impact of local topo-climatic factors. By incorporating a combination of sedimentological methods and relative dating of deposits, we aim to overcome the limitations of traditional geomorphological assessments and provide a more accurate reconstruction of the glacial landscape in this region.

## Study area

Babia Góra with the peak Diablak (1725 m a.s.l.) is the highest massif in the Western Flysch Carpathians and the Western Beskidy Mountains, located 45 km south of the front of the Carpathians and 50 km north-west (NW) from the Tatra Mountains (Fig. 1). The landscape of Babia Góra was developed within resistance 1 km thick Magura-type sandstones forming the syncline which overlies strongly folded, weak claystone/siltstone dominated flysch of the Hieroglyphic Beds (Książkiewicz 1971, 1983). Magura-type sandstones are Upper Eocene fine to medium-grained sandstones with a clay and silica-rich matrix, as well as coarse-grained sandstones with an iron-rich cement (Książkiewicz 1983, Jankowski, Garecka 2022).

Due to the Neogene tectonic uplift, Babia Góra stands out as a 10-km long isolated ridge with distinct local topography (up to 1 km) and strong structural asymmetry between northern precipitous anti-dip and gentle, southern dip slopes. The northern slope of the massif was shaped by one of the largest RSFs in the Western Carpathians (Alexandrowicz 1978, Kłapyta 2020, Łajczak 2023), with individual landforms reaching >2 km² in area (Kłapyta 2020, Kłapyta et al. 2025). The total area affected by the RSFs (9.5 km²) accounts for 77% of the sandstone cuesta slope area (Fig. 1C). Geomorphological mapping reveals the occurrence of all major types of RSFs, including rock slope deformations, rock slides and rock

avalanches, with a total volume of approximately 418 Mm$^3$ (Kłapyta et al. 2025). The RSF reflects a multistage evolutionary process with the most recent phase that began shortly after the last glacial maximum (LGM) and continued throughout the Holocene.

The landslide and fluvial morphology dominate the relief of the massif and was only slightly transformed by Quaternary glaciations. The only glacial cirque is incised into the north-western slope between Mt. Diablak (1725 m) and Mt. Kościółki (1620 m) (Łajczak 1981, 1998, 2023, Kłapyta 2020), while shallow cirque/niche was developed on the southern slope of Mt. Diablak at the Głodna Woda site (Fig. 2). Periglacial processes left a strong fingerprint in the highest part of the ridge in the altitudinal range of 1425–1725 m. These include a variety of periglacial landforms such as relict blockfields and blockstreams, cryoplanation terraces and small (1–2 m high) relict pronival ramparts (Jahn 1958, Ziętara 1989, Łajczak, Włoch 2004, Łajczak 2013, Kłapyta 2020).

Babia Góra is influenced by the preferential (65%) NW atmospheric circulation and moisture transport and due to its isolation acts as a distinct local topographic barrier (Fig. 1B). Due to orographic effect the windward northern slopes receive some of the highest precipitation in the region with an annual means exceeding 1450 mm and a maximum daily intensity >200 mm at an altitude of 1200 m (Obrębska-Starklowa 2004). The massif exhibits positive precipitation anomalies, with average precipitation totals of approximately 500 mm higher than the mean values recorded in the Western Carpathians in the period 1970–2000 (Fig. 1B). The prevailing winter winds from the south-west and south (Niedźwiedź et

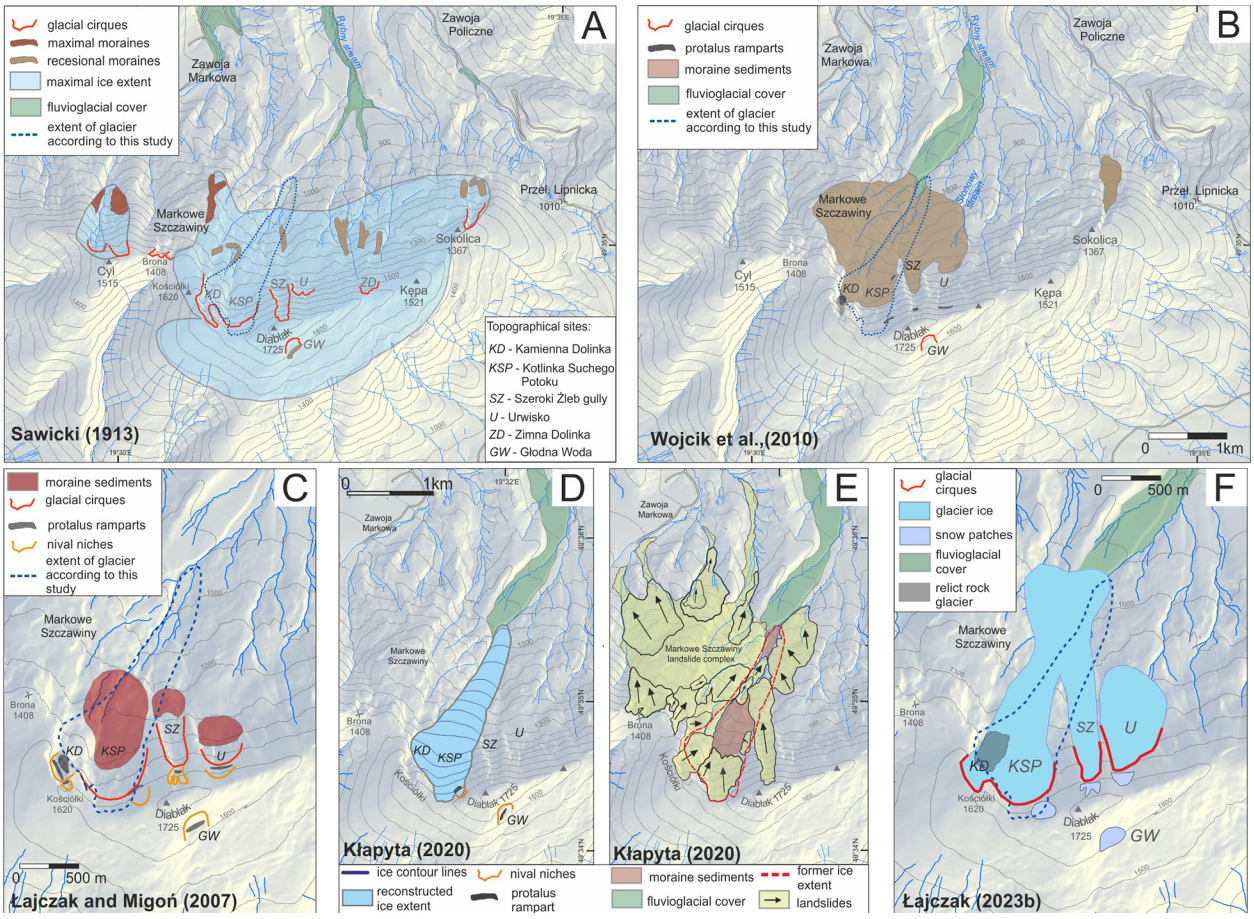


Fig. 2. The extent of glaciation in the Babia Góra massif according to previous studies. The extent of the Szumiąca Woda glacier presented in this study is marked with blue dashed lines. A – first geomorphological map of the Babia Góra massif according to Sawicki (1913). B – extent of moraine deposits according to Wójcik et al. (2010). C – extent of glacial and periglacial features according to Łajczak and Migoń (2007). D and E – reconstruction of glacier geometry and extent of moraines and landslide deposits according to Kłapyta (2020). F – extent of glaciers and snow patches during the last glaciation according to Łajczak (2023b).

al. 1985, Obrębska-Starklowa 2004) cause snow to be blown from the gentle southern slopes, leading to its redeposition by snow avalanches on the precipitous leeward slope, where the thickness of slope cover can exceed 5 m (Łajczak 2016). The MAAT ranges from 6°C at an elevation of 700 m a.s.l. to approximately 0°C at the Diablak summit (Obrębska-Starklowa 2004). Despite the negative annual temperatures, no evidence of contemporary permafrost was found in the summit area (Dobiński et al. 2016).

## Previous research and concepts on the glaciation of the Babia Góra.

The glaciation of Babia Góra was first suggested by Tietze (1888), although without supporting geomorphological evidence. The glacial cirque between Mt. Diablak and Mt. Kościółki was identified by Pax (1905) and Hanslik (1907). The first map of the glacial relief for this mountain range, published by Sawicki (1913), shows the locations of cirques, maximal and recessional moraines, as well as the extent of fluvioglacial covers (Fig. 2A). Sawicki also mentioned small-scale features such as roche moutonnées and glacially moulded bedrock, although these were not confirmed by subsequent research. He proposed the existence of an ice cap-type glaciation (approximately 10 km² in area) on both slopes of the massif during the maximal Würm glaciation with the lower limit of ice at 1050 m a.s.l. on the northern and 1400 m a.s.l. on the southern slope (Fig. 2A). The presence of smaller ice body was also stated on the northern slope of Mt. Mała Babia Góra (1515 m a.s.l.) (Fig. 2A). The presence of at least 12 small cirque/niche glaciers (300–400 m long and total area of 33 ha) were inferred between Mt. Sokolica and Mt. Mała Babia Góra during the recessional stage, which he attributed to the alpine Bühl stage (Fig. 2A). Sawicki (1913) also inferred the position of the ELA during the maximal glaciation at 1350–1400 m a.s.l. on the northern slope and 1550 m a.s.l. on the southern slope, and at 1440–1600 m a.s.l. during the recessional stage. Later, Klimaszewski (1948, 1952) associated these glacial stages with the maximal Pleistocene glaciation and the Last Glaciation.

Ziętara and Ziętara (1958) and Ziętara (1962), based on field mapping, largely rejected the concepts of Sawicki (1913) on the glacial genesis of many scars and hummocky boulder deposits and confirmed the dominance of landslide relief in the Babia Góra massif. While they did not rule out the possibility of glaciation, they found no glacial features, as the current morphology appeared to be entirely the result of intense landslide activity. Other authors (Starkel 1960, Książkiewicz 1963, 1966, Niemirowski 1963, Midowicz 1974) have also considered the possibility of glaciation of Babia Góra, but aside from brief descriptions, they did not provide documentation of their locations. According to Łajczak (1981, 1998) and Łajczak and Migoń (2007), three landslide scarps were reshaped by glacial erosion into glacial cirques, while six other scarps (including the Głodna Woda niche on the southern slope) were altered by nival processes (Fig. 2C). The limit of glaciers on the northern slope of Mt. Babia Góra was estimated at ca 1200 m a.s.l. and the largest ice body is 700 m long and 400 m wide (Fig. 2C). By contrast, Wójcik et al. (2010) presented a significantly broader distribution of glacial sediments, extending as low as 950 m a.s.l., covering a large portion of the northern slope of the Babia Góra massif, from the Markowe Szczawiny glade in the west to the Słonowy stream in the east (Fig. 2B). The presence of an isolated patch of moraine deposits was also reported below the Mt. Sokolica (1367 m a.s.l.).

Kłapyta (2020), based on LiDAR-supported geomorphological mapping and Schmidt-hammer relative age-dating, discovered remnants of terminal moraines in the Szumiąca Woda valley at 925 m a.s.l. and reconstructed the geometry of the paleoglacier (Fig. 2D). He found that a significant part of the former glacier extent was overprinted by mass movement processes. Łajczak (2023) revised his previous interpretation of the glacier's extent, lowering it to the level of the terminal moraines in the Szumiąca Woda valley. However, he proposed a different glacier geometry compared with Kłapyta (2020), including a right tributary from the Szeroki Żleb gully and a separate ice mass in the Urwisko area. Additionally, he proposed a reassessment of the origin of the previously identified Kościółki rock avalanche deposits in the Kamienna Dolinka valley (Alexandrowicz 1978, Ziętara 1989, Kłapyta 2020), suggesting that these deposits may actually represent a relict rock glacier that formed during deglaciation.

## Methods

### Geomorphological mapping and clast shape measurements

Geomorphological mapping of glacial landforms and sediments was carried out in the Szumiąca Woda Valley, situated in the central part of the Babia Góra massif, where evidence of past glaciation has been identified in previous studies (Wójcik et al. 2010, Kłapyta 2020, Łajczak 2023) (Fig. 1C). The fieldwork was complemented by the analysis of an airborne LiDAR-derived DEM with a 1-m horizontal resolution (GUGiK 2025) and colour orthophotos with a 25 cm pixel size, obtained from the Centre for Geodesy and Cartography of the Małopolska Council. Special attention was given to the geomorphological relationship between landslide features and presumed moraine landforms and sediments. For the delineation of cirques and their floors, topographic maps, DEM-derived hillslope maps, and contour lines were employed. Basic morphometric parameters of glacial cirque size and shape were automatically calculated using the ACME GIS toolbox (Spagnolo et al. 2017). In the glacial termination zone, the maximum size (*a*-axis) and position of the largest boulders were measured. Separately, the mean *a*- and *b*-axes was measured for 50 clasts of the moraine, landslide colluvia, and Holocene and Pleistocene alluvia. The longitudinal and transversal topographic profiles were generated using GIS software. A geomorphological map of the study area was produced and supplemented with the results from previous Schmidt-hammer dating campaigns (Kłapyta 2020, Kłapyta et al. 2025).

Due to the relatively weak geomorphological expression of glacial morphology, clast shape measurements (Glasser et al. 2009, Brook, Lukas

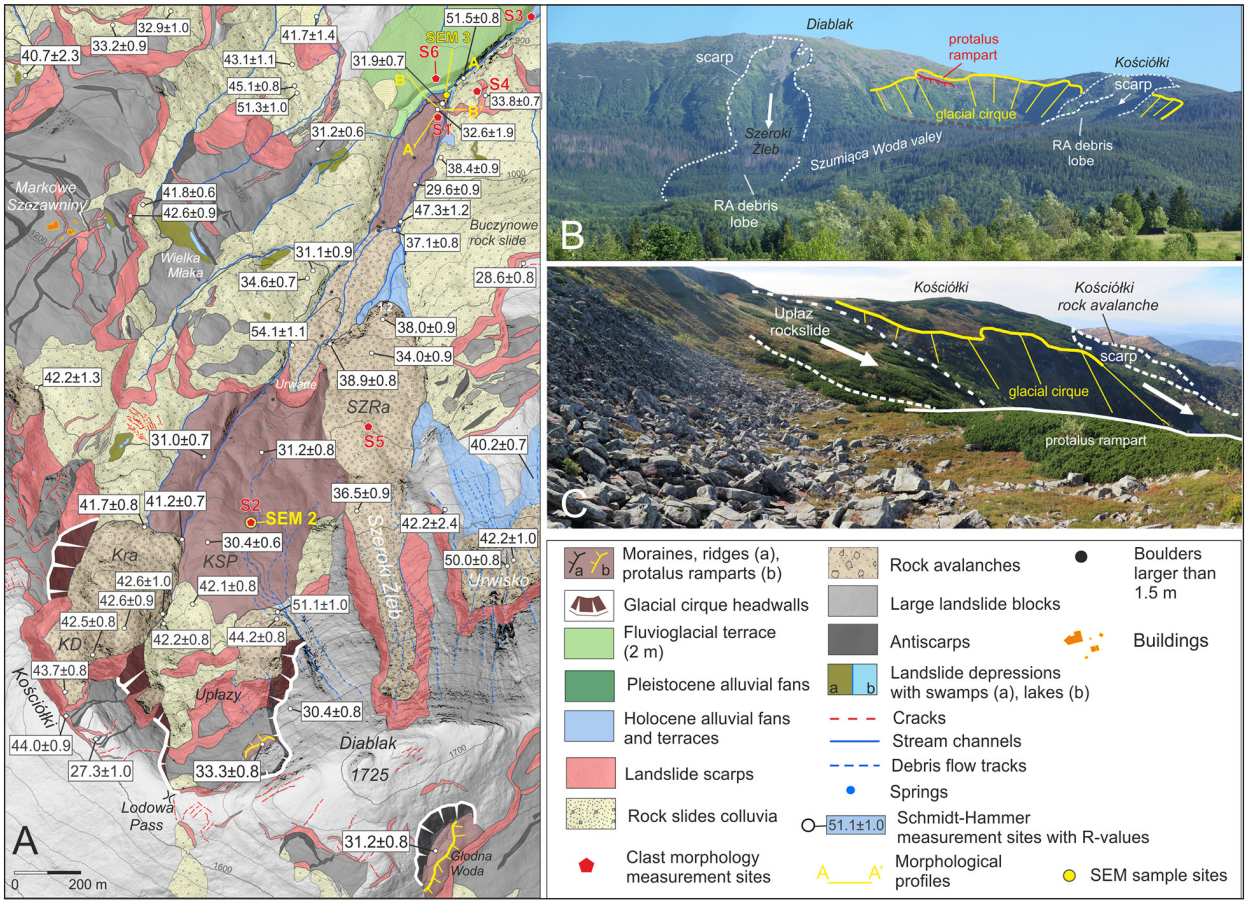


Fig. 3. Geomorphology of the Szumiąca Woda valley. A – Geomorphological map of the Szumiąca Woda valley with marked location and result of Schmidt-hammer measurements (Kłapyta et al. 2025). B – general view from the north on the headwall of the glacial cirque and scarps of rock avalanches. C – a headwall of the glacial cirque remodelled by RSF, view from the ridge of the Late Glacial protalus rampart. KD, Kamienna Dolinka valley; KRa, Kościółki Rock avalanche; KSP, Kotlinka Suchego Potoku; SZRa, Szeroki Żleb Rock avalanche.

2012) were conducted to support the interpretation of the mapped sediments. The clasts transported by glaciers typically exhibit a higher proportion of blade- and elongate-shaped forms, along with more pronounced rounding compared with those found in scree and landslide deposits. However, they are generally more angular than clasts from fluvial sediments (Lukas et al. 2013). Clast shape and roundness analyses were performed in the glacial termination zone (S1 site) and on the cirque floor (S2 site), and compared with control samples of known environments: fluvial alluvia in stream channel and Pleistocene alluvial fan (S3 site), rockslide (S4 site) and rock avalanche deposits (S5 site) (Fig. 3).

The measurements were conducted on Magura-type sandstones, the predominant lithology in the study area. For each site, the three orthogonal axes (*a*, *b* and *c*—long, intermediate and short) were measured for 50 clasts using a steel ruler. Clast roundness was visually assessed for each clast using a modified Powers (1953) scale. Tertiary diagrams following Sneed and Folk (1958) were created using the TRIPLOT Excel spreadsheet (Graham, Midgley 2000). The C40 index, which represents the percentage of clasts with a c/a axial ratio ≤0.4, was then calculated for each sample site. The C40 coefficient serves as an indicator of sediment transport types in glacial environments. Additionally, the RA ratio (percentage of angular and very angular clasts) and the RWR ratio (percentage of rounded to well-rounded clasts) were calculated for each site. The RA and RWR ratios help distinguish between sharp-edged clasts transported supraglacially and rock fragments that have undergone edge rounding during subglacial transport (Lukas et al. 2013). To better understand the transportation and depositional histories of the clasts, covariance plots were generated using both RA-C40 and RWR-C40 (Benn, Ballantyne 1994, Lukas et al. 2013). To examine the effects of flysch lithology on clast morphology in glaciated environments, the data from the Babia Góra massif (Kłapyta et al. 2025) were compared with clast morphology data from three mountain massifs in the Eastern Carpathians (Kłapyta et al. 2021b, 2022a, b), all of which built with flysch lithology.

## Microscopic analyses of quartz grains microtextures

Micromorphology of quartz sand grains (0.5–0.7 mm) was analysed at four sites (SEM 1–4) including landslide (SEM 1), moraine (SEM 2 and 3) and slope sediments (SEM 4) (Fig. 1). The samples were wetly sieved, digested in 10% HCL to remove carbonates and adhering particles, and washed at least four times in distilled water. At least 100 quartz grains were randomly collected from each sample under an optical microscope. Subsequently, each sample was analysed in terms of rounding and frosting of the grains' surface according to Cailleux (1942) with modifications of Mycielska-Dowgiałło and Woronko (1998) and with the application of 9° grain shape classification of Krumbein (1941). This method allows for recognition of the sedimentation environment by assigning each grain to one of the seven classes: angular and fresh (NU), aeolian well-rounded (RM), aqueous well-rounded (EL), aeolian moderately rounded (EM/RM), aqueous moderately rounded (EM/EL), broken (C) and intensively weathered (O) (Mycielska-Dowgiałło, Woronko 1998, Kalińska-Nartiša et al. 2017).

A total of 20 quartz grains were chosen randomly from each sample for microtextural analysis under the SEM Hitachi SU8600 at the Scanning Electron Microscopy and Microanalysis Laboratory at Jagiellonian University. This analysis presumes the visual observation of each grain and the recognition of microtextures, sets of which are interpreted as indicators of certain depositional environments, like fluvial, marine, aeolian or glacial (Mahaney 2002, Vos et al. 2014).

Each grain was first scanned and photographed in full size and then zoomed and analysed with the magnification between ×70 and 8000. Interpretation of the surface microtextures was performed according to Higgs (1979), Mahaney (2002), Woronko (2016) and Vos et al. (2014). We applied qualitative analysis to record the presence or lack of single microtextures on every grain. However, in the case of frost weathering microtextures (e.g. small and fresh conchoidal fractures with poor microrelief and fresh breakage blocks, Woronko, Hoch 2011) every noticed microtexture was counted. We used simple statistics

to combine the frequency of single microtextures. Special attention was given to discriminate fresh mechanically induced microtextures such as conchoidal fractures, linear steps, subparallel linear fractures, parallel ridges and arc-shaped steps. This freshness parameter was determined subjectively by comparing sharp (fresh) or etched/rounded (more weathered) edges of the fractures.

### Glacier reconstruction and ELA calculation

Glacier geometry was reconstructed on the basis of geomorphological relations using the GlaRe toolbox, a semi-automated GIS-based method (Pellitero et al. 2015). The mapped distribution of glacial sediments was also used to estimate the maximum ice extent in the Szumiąca Woda Valley, and the headwall of the glacial cirque marks the uppermost ice extent in the accumulation area. Ice thickness along the central flowline was calculated using a glacier profile model (Benn, Hulton 2010), with a calculated valley shape factor and basal shear stress (τb) values ranging from 20 kPa to 80 kPa, which are typical for low gradient and relatively shallow ice thickness (Žebre, Stepišnik 2014, Ruszkiczay-Rüdiger et al. 2022). Since the ice thickness was derived from the current bed topography, these values should be considered as minimum estimates.

The reconstructed glacier geometry was used for calculation of the former ELA, which serves as an important indicator of regional paleoclimatic conditions during the maximal glacial advance. Unlike older publications (Sawicki 1913), which relied on simple hypsometric relationships in calculating the ELA, we used the area altitude balance ratio (AABR) which is the most advanced method of ELA calculation. It takes into account the vertical distribution of the glacier surface and the mass balance ratio of 1.6, which is close to the global median value of monitored glaciers (1.56; Oien et al. 2020) and is commonly applied in previous studies across the Carpathian and Balkan region (Zasadni et al. 2020, Kłapyta et al. 2021a, b, Ruszkiczay-Rüdiger et al. 2021).

The calculation of ELA position based on the hypsometric characteristics of past glaciers is strongly influenced by local topo-climatic factors (shading, snow drift and avalanches), which can significantly affect the glacier mass balance (Mitchell 1996, Benn, Lehmkuhl 2000, Benn, Ballantyne 2005, Coleman et al. 2009) and significantly underestimates the regional ELA position (Dahl, Nesje 1992, Whalley 2009). To include a potential additional mass input to the glacier surface by snowblow and avalanches, we estimate a snow contribution area (sca) using the approach of Benn and Ballantyne (2005). The sca consists of the snowblow area, defined as the terrain located above AABR1.6 ELA, sloping towards the glacier and opposing slopes with inclinations of up to 10° (Sissons, Sutherland 1976, Coleman et al. 2009), as well as the avalanche area, defined as slopes around the glacier with inclinations >20° (Sissons, Sutherland 1976). The snowblow factor (SBF) and avalanche factor (AF), based on the ratio of the surface areas of the snowblow and avalanche areas to the total glacier surface, were adopted as measures of the additional contribution the glacier mass balance. Finally, we calculate scaELA, which includes inferred additional sca as the maximum estimate of climatic or regional ELA (Benn, Ballantyne 2005).

To measure the magnitude and imprint of glaciation (Kłapyta et al. 2023a), we calculate the Δridge-ELA index as the difference between the mean elevation of the ridge that limits the contributing area and the scaELA. This index was used to quantify the quantitative interrelation between Pleistocene ELA and mountain topography (Kłapyta et al. 2021b, 2022a, 2023a, b).

## Results

### Glacial landforms in the Babia Góra massif

One definite (grade 3), simple form glacial cirque (Kotlinka Suchego Potoku cirque) was distinguished in the headwaters of the Szumiąca Woda valley (Table 1). The cirque is northward oriented (17.5°) and 707 m long, 779 m wide and 369 m deep (Table 1). A sloping floor (mean 19°) is bounded by a 100 m high, moderately steep headwall with the maximal slope reaching 77°. The mean cirque area is 50 ha, the floor area is 20 ha and the perimeter averages 2896 m; 67% of the cirque area was reshaped by rock slides and rock avalanches in which rock scarps make retrogression of the cirque headwalls (Fig. 3). The Kościółki rock avalanche (0.16 $km^2$ in area, $2.64 \times 10^6$ $m^3$ volume) and the Upłazy rock slope

Table 1. Basic morphometric parameters of glacial cirque size and shapes in the Babia Góra massif.

| Parameter | | Unit | Kotlinka Suchego Potoku | Głodna Woda niche |
|---|---|---|---|---|
| Length | | [m] | 707 | 129 |
| Width | | | 779 | 183 |
| Elongation L/W | | [–] | 0.91 | 0.70 |
| Perimeter | | [m] | 2896 | 683 |
| Circularity | | [–] | 1.16 | 1.28 |
| Area | Entire cirque | [ha] | 49.80 | 0.23 |
| | Cirque floor | | 20.300 | 0.095 |
| Bottom area/cirque area | | [%] | 40.9 | 41.0 |
| Median aspect of cirque axis | | [°] | 17.5 | 156 |
| Maximal cirque slope | | | 77 | 51 |
| Maximal elevation of cirque edge | | [m a.s.l.] | 1664 | 1671 |
| Minimal elevation of cirque bottom | | | 1295 | 1598 |
| Mean elevation of cirque floor | | | 1357 | 1620 |
| Height range | | [m] | 369 | 73 |
| Length/height range | | [–] | 1.91 | 1.77 |
| Grade | | | 4 | 5 |

failure (RSF) complex (0.22 km$^2$ in area, 4 × 10$^6$ m$^3$ volume) (Kłapyta et al. 2025) were formed due to the collapse of the cirque headwalls after deglaciation as is indicated by Schmidt-hammer weathering indexes (Fig. 3). The area above the cirque headwall is prone to rock slope deformations which is supported by the presence of tension cracks, double-crested ridge, downhill- and uphill-facing scarps (antiscarps) (Fig. 3A). The mean floor altitude of the cirque is 1357 m a.s.l. with moraine deposits that are preserved beyond the landside colluvia in the northernmost part of the cirque. Their SH weathering index (R-value = 30.4–31.2) (Kłapyta et al. 2025) supports its much older age than the surrounding RSFs (R-value = 41.2–44.2; Fig. 3).

Small (125 m long and 2 m high), curved ridge of the protalus/pronival rampart (Hedding, Sumner 2013) was formed at the margin of a shallow hollow located in the SE corner of the cirque headwall at 1585 m a.s.l. (Fig. 3). The feature is built with angular-shaped clasts and, according to SH data, was formed during the Late Glacial (R-value = 33.3) (Kłapyta et al. 2025).

On the southern slope of Mt. Diablak in the Głodna Woda area, the marginal cirque/nival niche was developed due to its small size (129 m long, 183 m width), gentle headwall with the maximal slope of 51° and rounded crest (Table 1); its glacial origin is debatable. Due to its small size and shallow form, it is rather nival than glacial landform. This hollow is closed at 1620 m a.s.l. with a 300-m long debris ridge, where sandstone boulder exhibits the same weathering index (R-value = 31.2) as moraine covers in the Szumiąca Woda valley (Fig. 3).

The thickness of the moraine deposits on the northern slope of the massif can be estimated below the cirque threshold in the scarp of the historical Urwane rock avalanche (1858 CE), where a 2–5 m thick diamict, consisting of a sandy-silty matrix with cobble- to boulder-sized clasts are resting on bedrock built with Magura beds (Fig. 3). Downslope, large (>2 m), subrounded boulders are scattered throughout the body of the rock avalanche, particularly along its front, where one of the largest boulders (2.3–2.5 m) has been documented (Figs 3 and 4A).

The terminal moraine zone is exposed at an altitude of 925 m a.s.l., at the base of Szumiąca Woda Valley, where a 20 m high latero-frontal moraine rises above the flat valley floor (Fig. 4). The maximum extent of the glacial deposits is clearly marked by a lithologic contrast between the local bedrock, consisting of weak claystone and siltstone-dominated, thin-bedded flysch of the Hieroglyphic Beds, and the moraine material, which is primarily composed of Magura-type sandstone boulders and cobbles (Fig. 4). The latero-frontal moraines form a steep (20–30°) ridge, with the inner zone characterised by debris-rich hummocky topography typical of debris-covered glaciers. This topography extends continuously from the terminal moraines to the front of the Urwane rock avalanche (Fig. 3).The terminal moraines pass into a 2 m high terrace built with

sandstone sandy gravels with maximal cobbles of size ~1 m (Fig. 4). We link this feature as a remnant of fluvioglacial cover formed during the maximal extent of glaciation (Fig. 3). This terrace is nested within older, Pleistocene alluvial covers which form distinct alluvial fan situated at elevations from 12 m to 20 m above the present-day channel (Fig. 3). The fan is built with 1.6 m thick well-rounded sandy gravels (with maximal clast dimension of 0.15 m) which were deposited on bedrock built with Hieroglyphic Beds. The remnants of the terminal moraine zone are overprinted by rock slide colluvia from both the slopes of the valley. Their SH weathering index (R-value = 34.8–38.4) (Kłapyta et al. 2025) supports its much younger age in relation to moraine deposits (Fig. 3).

The moraine sediments consist of matrix-supported, subrounded and subangular boulders and cobbles (1–1.5 m in diameter), with the largest perched boulders reaching up to ~3 m (Figs 4 and 5). The mean clast dimensions found in the moraine deposits (a = 1.3 m, b = 0.8 m) is much higher than measured for the Holocene alluvia (a = 0.67 m, b = 0.46), Pleistocene alluvial fan (a = 0.09 m, b = 0.06 m), Szeroki Żleb rock avalanche (a = 0.75 m, b = 0.46) and Buczynowe rockslide (a = 0.47 m, b = 0.28) (Fig. 5).

Moraine deposits in the Babia Góra massif are built with sandstones with the dominance of partially rounded (20–60%) and slightly angular clasts (20–30%), with a smaller proportion of angular and rounded clasts (up to 5–10%) (Fig. 5). The higher angularity was found in the terminal moraine zone (RA = 38%, S1 site), which could be linked with a higher proportion of passively transported supraglacial debris in comparison with the cirque area (RA = 4%, S2) (Fig. 5). The

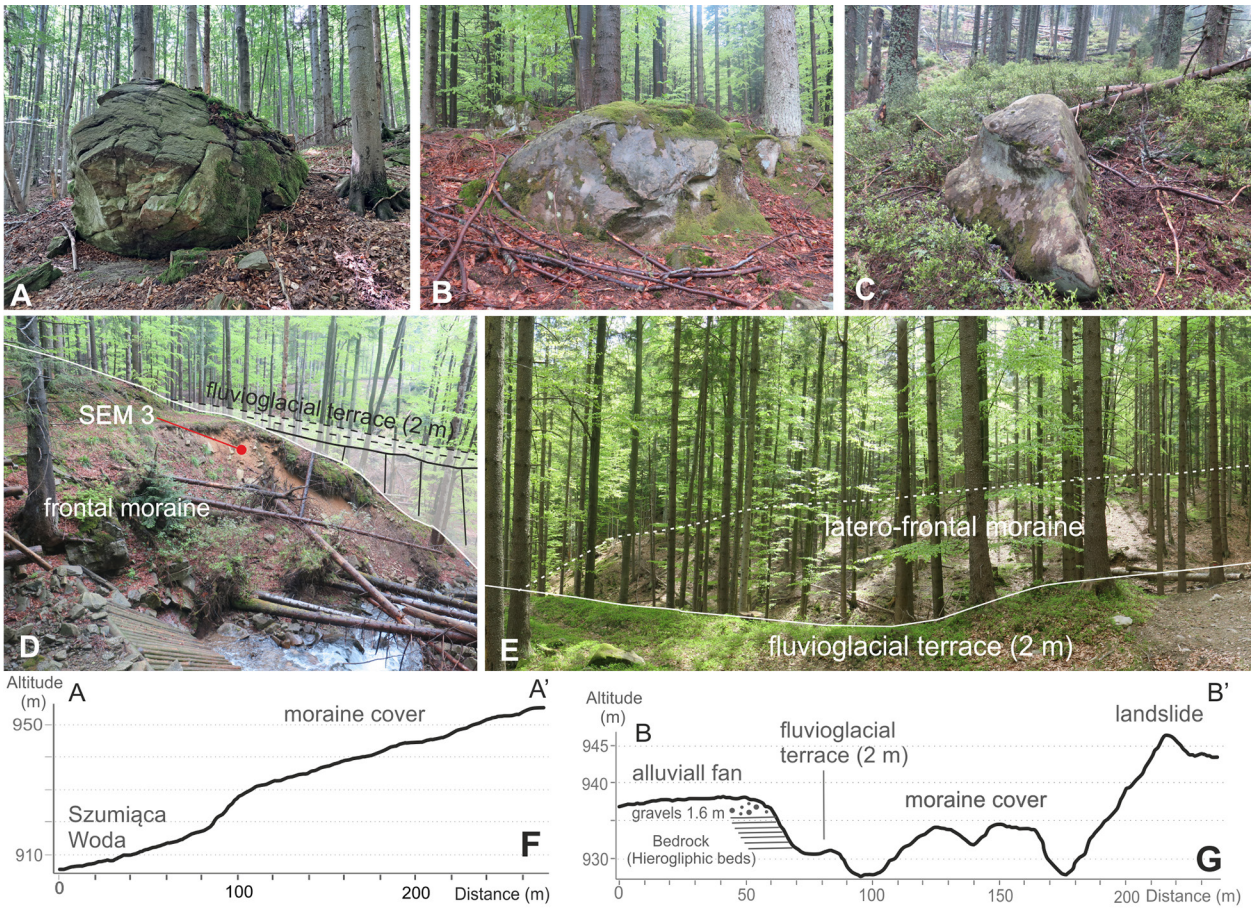


Fig. 4. Moraine landforms and sediments in the Babia Góra massif. A–C – examples of large surface boulders at the surface of moraine covers (for location see Fig. 3A). D – a steep 15 m high front of moraines in the Szumiąca Woda valley (view from the east). E – laterofrontal moraines in the Szumiąca Woda valley (view from the west). F – longitudinal profile along the axis of the Szumiąca Woda valley (for location see Fig. 3A). G – transversal profile across moraine covers in the Szumiąca Woda valley (for location see Fig. 3A).

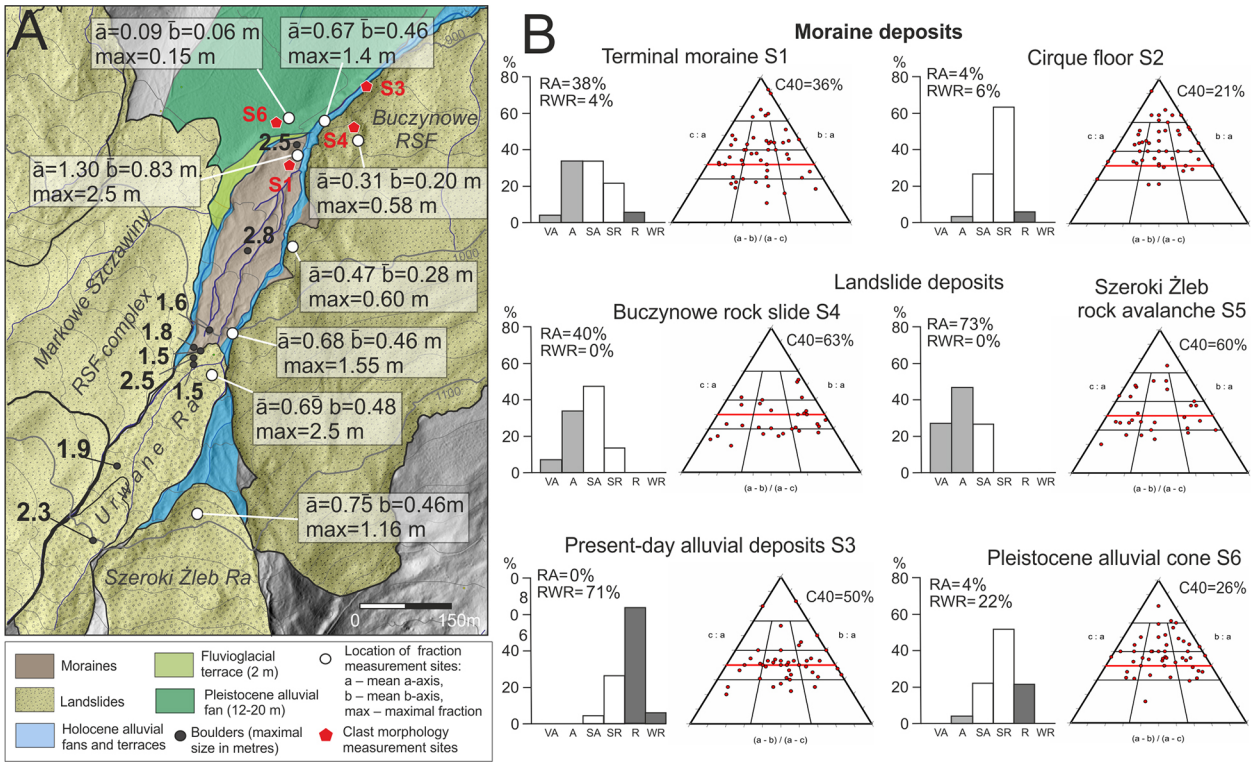


Fig. 5. Sedimentological analysis of clast in the Szumiąca Woda Valley. A – boulder and clast fraction measurements in the terminal moraine zone in the Szumiąca Woda valley. B – roundness (histograms) and clast shape data (ternary diagrams) for sampled sites in the Szumiąca Woda area. Red solid line marks the position of C40. Site locations are depicted in Fig. 3. RA and C40 are defined in the text.

C40 indices for moraine deposits range between 21% and 36%, thus aggregating predominantly compact blade and compact elongate clasts. Notably higher C40 indexes (60–63%) were calculated for landslide deposits and present-day fluvial gravels (50%) (Fig. 5), indicating the domination of platy clasts. The difference between moraine and other sedimentary environments is even better visible when taking the RWR ratio (Fig. 5). The RWR values are low for moraines (mean 5%), very low for landslides (mean 0%) and high (71%) for fluvial sediments.

## Micromorphology of quartz grains

Microscopic analyses of quartz grains (0.5–0.7 mm) indicate that weathered grains (O type) with medium to high relief comprise approximately 80% of each sample (Fig. 6). These grains exhibit chemically altered surfaces, characterised by dissolution surfaces, and microtextures such as solution pits, solution crevasses and amorphous silica precipitations (Figs 6A and 7A). By contrast, fresh and angular grains (NU type), and cracked grains (C type) account for 4.5–12% of the studied samples (Figs 6 and 7D). NU-type grains are more common (8.5%) in the SEM 2 sample, while C-type grains (12%) dominate in the SEM 3 sample.

Abrasion microtextures are frequently observed in all samples, with their freshness and preservation serving as key differentiators between the samples (Figs 7B–H and 7K). The presence of mechanically induced microtextures is particularly evident in SEM 1–3 samples. These features are primarily seen as large conchoidal fractures, often forming cleavage surfaces (cf. Higgs 1979, Vos et al. 2014, Fig. 7I). Linear steps, arc-shaped steps and subparallel linear fractures are also commonly seen. Although fresh surface is observed on 20–50% of the grains depending on all the samples, single fresh conchoidal fractures and breakage blocks are noticed in 80% of the SEM 3 sample. This sample also exhibits the highest proportion of linear steps, micro steps, cracks, sawtooth fractures and small breakage blocks (Figs 7G–I). Notably, small breakage blocks (<10 μm) predominate in this sample,

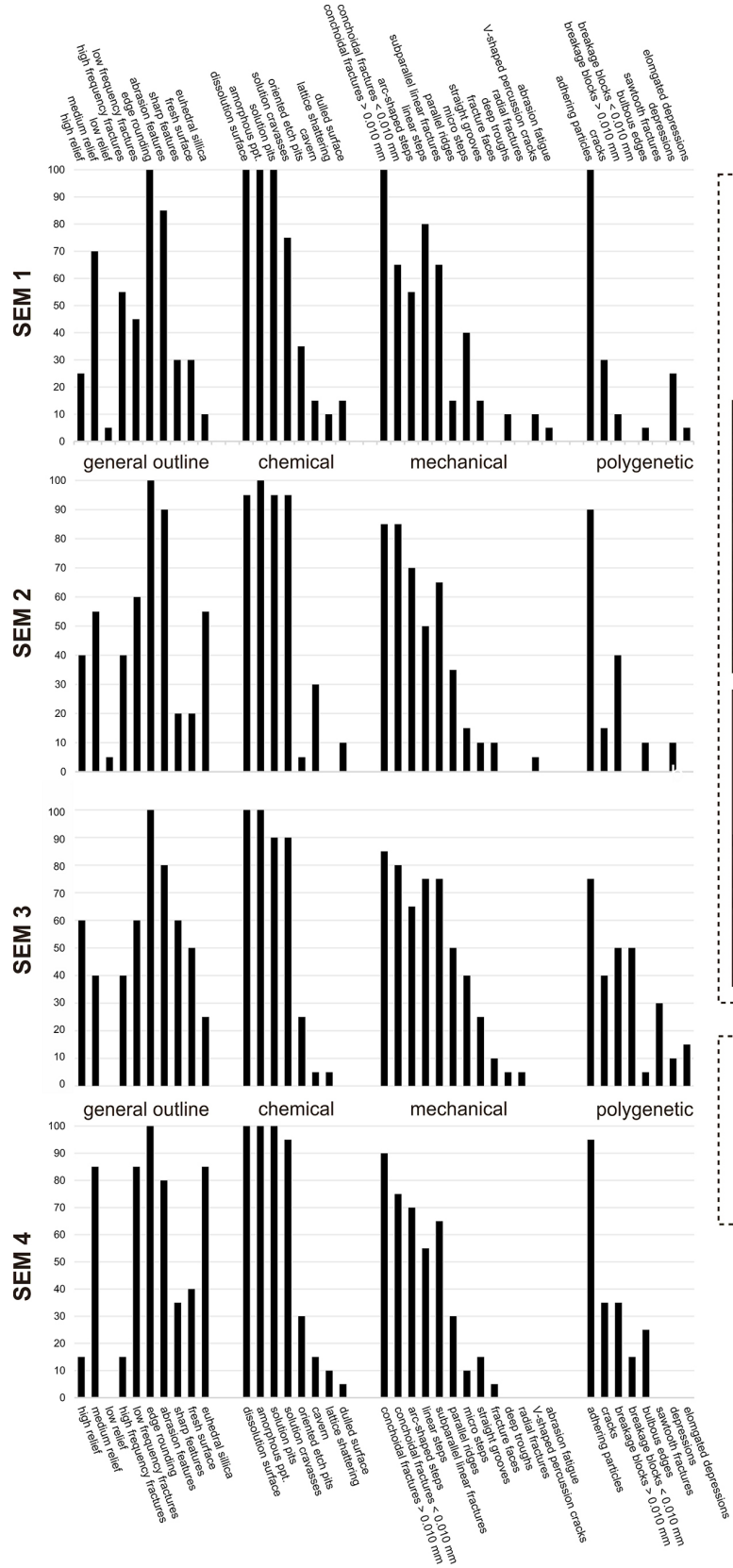


**frost weathering intensity**

| sample | number of grains | number of fresh microtextures (conchoidal fractures + breakage blocks) |
|---|---|---|
| SEM I | 3 | 7 |
| SEM II | 7 | 24 |
| SEM III | 16 | 63 |
| SEM IV | 8 | 26 |

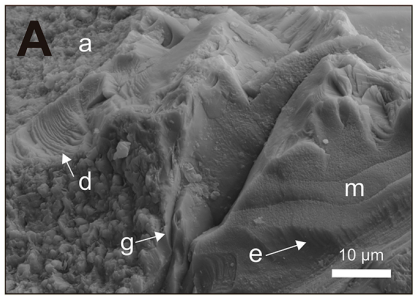


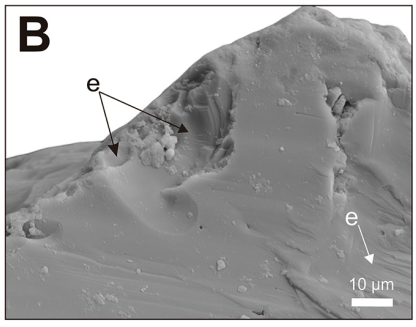


**rounding and frosting**

| Sample | Type of grain (%) NU | RM | EL | EM/RM | EM/EL | O | C |
|---|---|---|---|---|---|---|---|
| SEM I | 6 | 0 | 0 | 4 | 0 | 84 | 6 |
| SEM II | 8,5 | 0 | 0 | 0 | 0 | 83 | 8,5 |
| SEM III | 4,5 | 0 | 0 | 2,5 | 1 | 80 | 12 |
| SEM IV | 6 | 0 | 0 | 0 | 5 | 81 | 8 |

Fig. 6. Variations of observed microtextures according to general features and genetic processes. Frost weathering microtextures depicted on micrographs A and B (explanations as in Fig. 7) were counted according to Woronko and Hoch (2011). Rounding and frosting types were according to Cailleux (1942) with modifications of Mycielska-Dowgiałło and Woronko (1998).

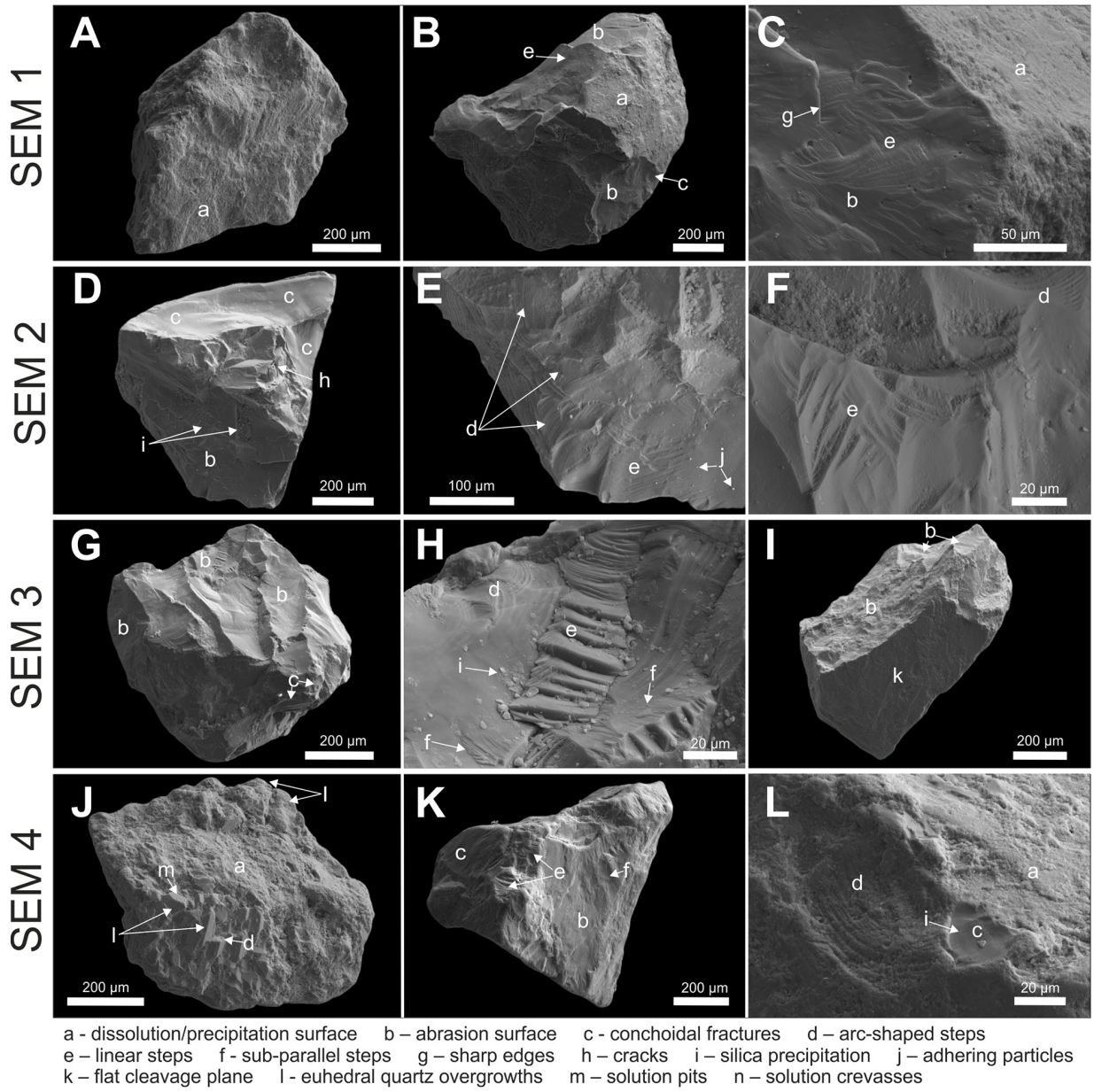


Fig. 7. Micrographs of quartz grains: A – subrounded grain with medium relief and chemically weathered surface; B – subrounded grain with high relief and dissolution/precipitation surface overprinted by mechanical weathering; C – the contact zone between the older chemically weathered surface and younger abrasion surface of large fracture; D – angular grain with high relief and fresh surface. The grain is considered crushed during glacial transport due to almost complete reshaping of its surface by large conchoidal fractures and other abrasion features; E – details of abrasion features of the grain shown in D; F – details of probably older abrasion features. Edges of the fractures are slightly rounded, and precipitation features are frequent; G – glacially abraded/crushed grain with high relief and fresh surface. Elongated depressions created probably along the crystals' contacts and numerous abrasion features are interpreted as the effects of glacial abrasion; H – details of the upper part of the grain in G showing the irregular abrasion patterns; I – angular grain with high relief. Abrasion surfaces are of different freshness – more weathered and probably older (upper left), adjoin fresh and sharper ones (top centre). The flat cleavage plane propagated along the crystal structure and is the most weathered; J – subrounded grain with medium relief and euhedral quartz overgrowths of different freshness, which are slightly altered due to chemical etching and mechanical weathering; K – subrounded grain with high relief. Although grain represents in situ slope covers, many abrasion features can be seen. They are subordinate to large conchoidal fractures and possibly arise during the separation of grain from the host rock; L – arc-shaped steps covered by solution/precipitation features. The relief is rejuvenated by a relatively fresh conchoidal fracture, which is slightly etched and precipitated by amorphous silica.

whereas they are nearly absent in the others (Fig. 6). Yet, in all samples, most of the fractures are etched with slightly rounded edges (Fig. 7C). In a few grains, abrasion microtextures represent the oldest microtextures observed within the samples, as they are partially masked by dissolution surface (Fig. 7L).

The frequency of certain other microtextures also differentiates the samples. For example, grains with euhedral silica (Fig. 7J) display significant variation across the samples, ranging from 10% in SEM 1 sample to 85% in SEM 4 sample. Even among the moraine samples, the difference is substantial, reaching 30%. It is also worth noting that V-shaped percussion cracks are present in 5–10% of the grains in SEM 3 sample. However, microtextures of aeolian origin, such as crescentic percussion marks and upturned plates, are absent across all samples.

## Glacier reconstruction and ELA calculation

The Szumiąca Woda cirque-valley glacier was reconstructed on the northern slope of the Babia Góra (Fig. 8). The mean glacier length was 2.2 km and its area (0.87 km$^2$) was <1 km$^2$. The glacier terminated at 930 m a.s.l., and its elevation range was 700 m. The area-averaged glacier thickness was 19 m, whereas the maximum thickness reached 47 m in the cirque area (Fig. 8B). The ELA (AABR1.6) of the reconstructed palaeoglacier was at 1272 m a.s.l., which is slightly lower compared with the value obtained by applying the AAR 0.5 method (1294 m a.s.l.).

The total potential snowblow area was 0.55 km$^2$ and encompasses gently sloping southern slopes between Mt. Diablak and Kościółki (Fig. 8A). The SBF was similar to the area of the reconstructed glacier (0.79), thus the additional

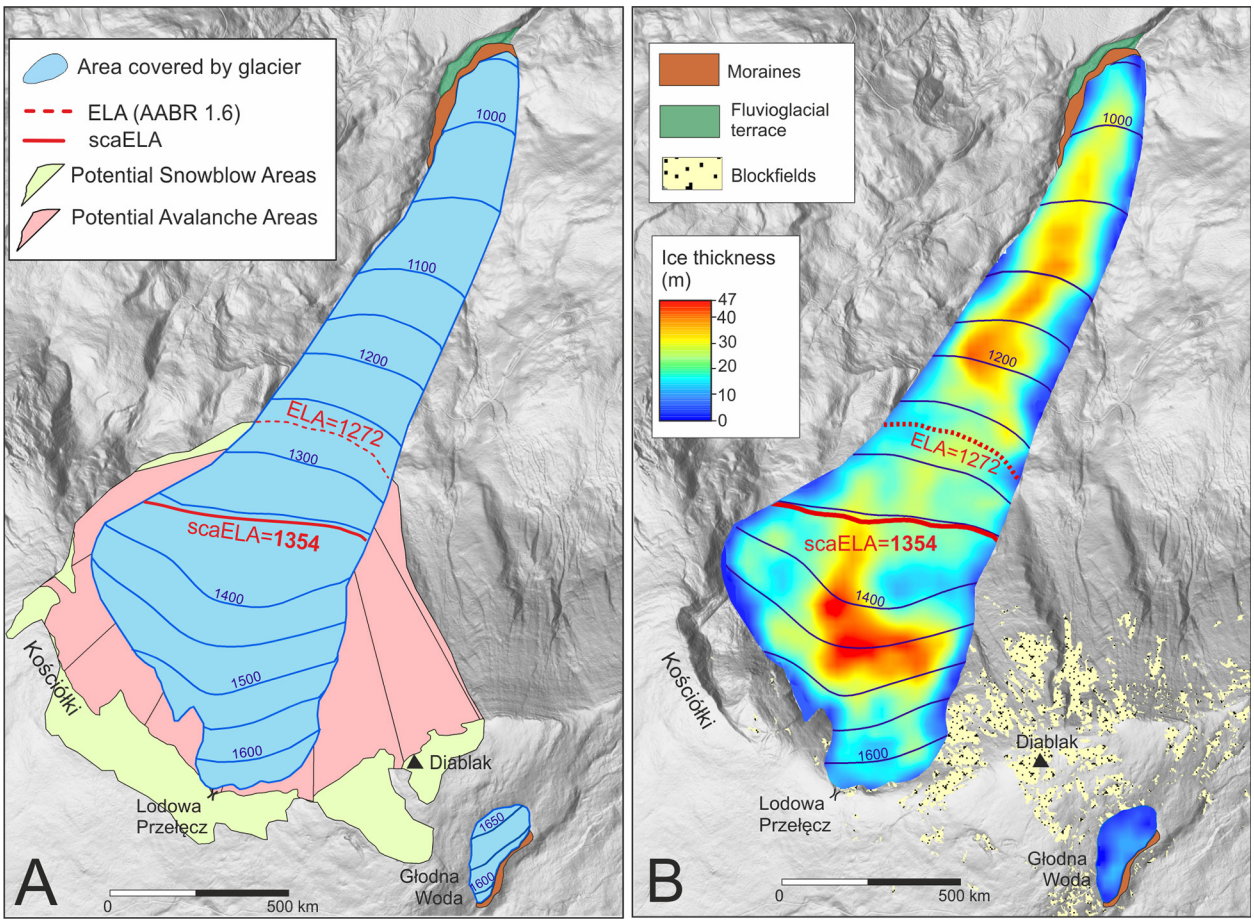


Fig. 8. Glacier and equilibrium line altitude (ELA) reconstruction of the paleoglacier in the Szumiąca Woda valley and snow-ice body in the Głodna Woda area. A – distribution of potential snowblow areas and potential avalanche areas of the Szumiąca Woda palaeoglacier. The position of ELA area altitude balance ratio (AABR1.6) and scaELA are marked in dashed and solid red lines, respectively. B – glacier thickness of the palaeoglaciers.

snowblow delivery could significantly control the size of the glaciers and the ELA position. The snow contribution by avalanches was less important (0.34 km$^2$) as the AF was 0.38. The inclusion of sca in the ELA calculation (Benn, Ballantyne 2005, Kłapyta et al. 2022a, b) gives the mean scaELA at 1354 m a.s.l., which is 82 m higher than the AABR1.6 ELA. The difference between the mean elevation of the ridge that limits the contributing area of the glacier (1634 m) and the mean ELA of the glacier (Δridge-ELA) was 280 m.

## Discussion

### Glacier landforms in the Babia Góra massif in relation to the previous concepts

The results of geomorphological and sedimentological analysis confirm the legacy of Pleistocene glaciation in the Babia Góra massif. Detailed mapping of the Szumiąca Woda valley reveals that 68% (87 ha) of the total glaciated area has been affected by RSFs, with glacial deposits preserved only in two altitudinal zones: 925–1000 m and 1180–1380 m (Figs 1 and 3). The position of the glacial cirque between Mt. Diablak and Kościółki aligns with all previous interpretations, dating back to the earliest observations (Pax 1905, Hanslik 1907, Sawicki 1913).

By contrast, we cannot support the presence of a glacial cirque in the Szeroki Żleb and Urwisko areas (Łajczak, Migoń 2007, Łajczak 2023, Łajczak et al. 2023). In pioneer studies (Sawicki 1913) the Szeroki Żleb area was even thought as glacial through. The Szeroki Żleb is a 650 m long, 270 m wide, steeply sloped (55-65°) rock cavity with a very high L/W ratio of 2.41, which is uncommon in the morphometry of glacial cirques (Fig. 3B). The typical mean L/W ratio for cirques is close to 1 (Evans 2006). In the Carpathians, the mean L/W ratio is 0.9 for all 631 cirques in Romania (Mîndrescu, Evans 2014) and 0.94 for the 214 cirques in the Eastern Carpathians (Kłapyta et al. 2023a). In the case of the Kotlinka Suchego Potoku cirque and Głodna Woda niche, these ratios are 0.91 and 0.7, respectively (Table 1). Below the Szeroki Żleb rock cavity, a 700 m long tongue-shaped debris piles the floor of the Szumiąca Woda valley. The high RA, C40 and low RWR indexes measured for debris support the RSF genesis of this feature, whereas the Schmidt-hammer results (R-value = 34–38) indicate its much younger age in comparison with moraine covers (R-value = 30.4–31.2; Fig. 3). This indicates that the Szeroki Żleb represents a rock avalanche scar which was formed after deglaciation of the study area (Kłapyta et al. 2025). Its RSF origin is additionally supported by the mean volume of the debris accumulation (4.36 M m$^3$), which fits well with the volume of the RSF scarp (4.38 M m$^3$).

The Urwisko is a steep scarp of old landslide, which was remodelled by succeeding rock avalanches (Fig. 3) without signs of cirque floor and ice marginal features. This feature is outsloping (>20°) and shallow landform that did not favour accumulation by snow avalanches at its steep bottom (1240–1260 m a.s.l.), which was located below the local glacier equilibrium line.

### Palaeoclimate implications

The Babia Góra massif was the northernmost glaciated area in the Carpathians (49°34′N) (Fig. 1A). with the reconstructed climatic ELA at 1354 m a.s.l. This value is the same as the mean elevation of the cirque floor (1357 m a.s.l.) obtained in this study. According to Mîndrescu and Evans (2014), the mean elevation of the cirque floor could be used as a proxy for the lowest ELA during maximum glaciation; thus, our result strengthens the palaeoclimate significance of this proxy for ELA estimation. Despite its marginal position relative to the mountain front and the strong orographic effect that promoted high precipitation, the reconstructed climatic ELA in the Babia Góra massif (1354 m a.s.l.) was not the lowest within the range. The lowest regional climatic ELA in the entire Carpathian arc (1289 m and 1352 m) was placed in the Polonyna Rivna and Borzhava, respectively, located in the NW part of the Eastern Carpathians (Fig. 1A). This local phenomenon was linked with the combined effects of relatively cold air temperatures and orographic-induced precipitation, which was amplified by the effect of colder winters and shorter ablation seasons in the more continental interior (Kłapyta et al. 2022a, b, 2023a, b).

According to previous studies (Sawicki 1913, Pawłowski 1933, 1936, Wójcik 1994), evidence of former glaciation in the Western Flysch

Carpathians has been documented also in the Mt. Pilsko massif (1557 m a.s.l.), located 16 km to the west of the Babia Góra massif (Fig. 1B) (Sikora, Żytko 1960). These concepts were further questioned by Ziętara (1962) and Łajczak (1998, 2015), who attributed the morphology in the Hala Miziowa area with RSF activity. These observations are in line with LiDAR data which confirm that local terrain depression enclosed by an arcuate ridge is the upper part of the large (70 ha) rockslide descending to the Kamienna valley.

In the Western Carpathians, evidence of Pleistocene glaciation has been identified in five mountain massifs (Fig. 1B; Table 2). However, except for the Tatra and Low Tatra Mountains, where valley-type glaciation was dominant (Lukniš 1964, Zasadni, Kłapyta 2014, 2022, Kłapyta, Zasadni 2018, Zasadni et al. 2021, Pyrda 2025), the Malá and Veľká Fatra Mountains were primarily affected by marginal and cirque-type glaciation (Paulo 1937). In the latter regions, glaciation was largely influenced by local topography, which favoured the accumulation of windblown snow in the lee-side cirques. The spatial patterns of paleo-ELA suggest a dominant western moisture transport to the Tatra Mountains during the Last Glacial Maximum (Zasadni et al. 2018). A distinct eastward rise in the ELA of 100–130 m was observed over a distance of 40 km between the Western (1450 m) and High Tatras (1580 m). This pattern is in line with an ELA position in the Malá Fatra Mountains located ca 60 km to the west, which was inferred at 1392 m a.s.l. (Paulo 1937, Table 2). New data from this study indicate an additional southward rising ELA trend in the Western Carpathians, spanning from the Babia Góra massif (1354 m a.s.l.) to the Western Tatras (1450 m a.s.l.; Zasadni et al. 2018) and the Low Tatra Mountains (1431 m a.s.l.; Pyrda 2025). However, this last value may be underestimated due to the lack of inclusion of additional sca in ELA calculation (Kłapyta 2022).

Mutual relationships between the ELA and mountain hypsometry can quantitatively define the degree of glacial relief development (Kłapyta et al. 2023a). Studies in the Eastern Carpathians (Kłapyta et al. 2023a) suggest that mountain-type glaciation could have been initiated in massifs standing at least 100 m above the ELA. In the Babia Góra massif, the Δridge-ELA reaches 280 m, indicating the presence of an intermediate level of glaciation. This is characterised by cirque and valley glaciers exclusively on the northern slopes, as well as small cirque glaciers on the southern slope. The glaciation asymmetry is pronounced, and the cirques predominantly belong to type 3 (definite). In the Eastern Carpathians, this level of glaciation has been observed in the Svydovets massif, the Pietros group of the Chornohora Mountains and the Maramureş Mountains (Kłapyta et al. 2021a, b, 2023a, b, 2024). The best analogues were the Jupania paleoglacier in the Maramureş Mountains, which exhibit similar area and length (area 0.85 km$^2$, 1.7 km long) (Kłapyta et al. 2023b, 2024).

In this context, the presence of a small nival field in the Głodna Woda area appears to be supported by the local topo-climatic conditions, which favour snow accumulation in a depression located on the leeward side. The shallow niche could have resulted from nival remodelling of an older landslide scarp. These specific local topo-climatic conditions are evident even under current climatic conditions, with the Głodna Woda depression, despite its southern exposure, hosting the largest and longest-lasting snow patches in the entire massif (Łajczak 2016).

## Glacial impact on moraine clast reworking in the flysch area

Sandstones are highly susceptible to glacial abrasion compared with crystalline rocks, but in the moraine deposits composed of these rocks,

Table 2. Late Pleistocene ELA position in the Western Carpathians (AABR, area altitude balance ratio).

| Mountain massif | Altitude | ELA position | Method | Reference |
|---|---|---|---|---|
| | [m a.s.l.] | | | |
| Babia Góra | 1725 | 1354 | AABR1.6 | This study |
| Malá Fatra | 1708 | 1392 | Cirque floors | Paulo (1937) |
| Western Tatras | 2250 | 1450 | AABR1.6 | Zasadni et al. (2008) |
| High Tatras | 2655 | 1580 | AABR1.6 | Zasadni et al. (2008) |
| Low Tatras | 2043 | 1431 | AABR1.6 | Pyrda (2025) |

very low values of the C40 index (spheroidal and isometric forms resulting from abrasion) were not observed. This can be explained by the continuous fracturing of the rock particles, which commonly occurs during glacial transport and abrasion (Lukas et al. 2013). Granulometric analysis of fine matrix (Kłapyta et al. 2025) reveals that moraines have the highest mean grain size (Mz) and the lowest content of the finest fractions (~40%) in comparison with the scree, landslide and fluvial sediments.

Covariance plots for the moraine deposits in flysch lithology show that debris cascade in the Babia Góra massif built with Magura type sandstone is similar to the flysch massifs in the Eastern Carpathians and correspond well with the model of debris cascade model in glaciated areas built with highly anisotropic rocks (Lukas et al. 2013) (Fig. 9). The differences between glacial sediments and fluvial and slope deposits is related to rounding (RA index). A clear evidence of actively transported clasts (subglacial) was found in the cirque (S2 site, Figs 3 and 9) at a distance of ~800 m from the upper rim of the cirque. Similarly, the lowest RA (0–5%) and the highest RWR (20–30%) values were obtained in the Polonina Rivna and Borzhava for moraine sites located 0.7–1.0 km down valley from the cirque headwalls; however, the minimum distance of clast reworking in the flysch part of the Eastern Carpathians was noticed at 250–300 m (Kłapyta et al. 2022). The markedly higher RA values (~40%) typical for passive glacial transport were found in the terminal moraine zone, which could be linked with the presence of supraglacial debris cover (Fig. 9) and the hummocky topography.

## Glacial impact on quartz grain reworking in the flysch area.

This study is the first application of SEM analysis of quartz grain microtextures in a glaciated flysch area of the Carpathians. The recognition of glacial activity based on changes in the grains' relief is possible when pre-glacial processes are revealed and compared with microtextures that resulted from glacial abrasion during the transport.

This study reveals that before the glacial reworking, quartz grains were subjected to intensive chemical weathering and physical disintegration. Chemical alteration of the grains led to the etching and precipitation of amorphous silica (Figs 7A, 7J and 7O), which may have undergone in marine environment in more alkaline conditions, enhancing silica solubility (Wray, Sauro 2017) or within the subtidal zone where oriented etch pits (up to 35% in SEM 1, Fig. 6) may arise (Vos et al. 2014). Nevertheless, the possibility of quartz dissolution within soil profiles cannot be excluded. Evidence of quartz etching has been reported

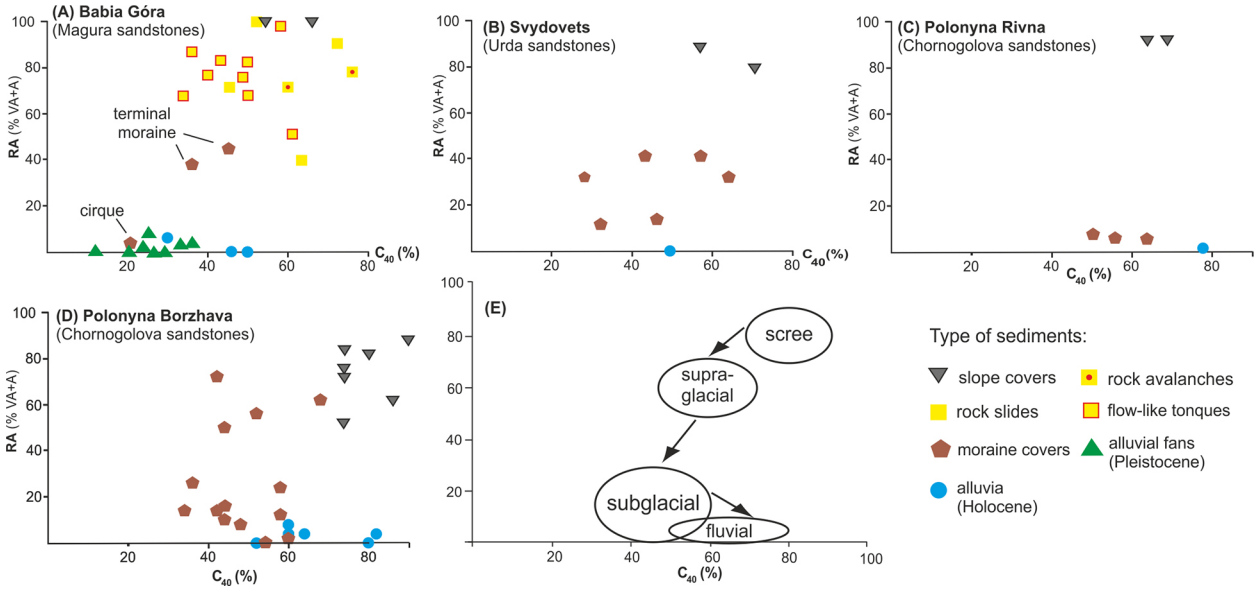


Fig. 9. Covariance plots for the moraine deposits in flysch lithology in the Babia Góra massif (A – Kłapyta et al. 2025), Svydovets (B – Kłapyta et al. 2021a, b, Supp. data 1), Polonyna Rivna and Borzhava (C and D – Kłapyta et al. 2022a, b) in comparison with the debris cascade model in glaciated areas built with highly anisotropic rocks (E – Lukas et al. 2013). Each plotted point represents a sample group of 50 clasts.

in regions characterised by tropical climates (e.g. Doornkamp, Krinsley 1971, Pye 1983). According to Pye and Mazzullo (1994), under such environmental conditions – specifically within podzolic soils – quartz etching may proceed relatively rapidly, occurring within <8000 years, particularly in the presence of high rainfall, low pH (3–4.5) and elevated concentrations of organic acids. Conversely, in such settings, the rate of quartz loss can also be significantly lower, as exemplified by the slow dissolution observed in saprolites studied by Schulz and White (1999). Quartz dissolution can also occur in temperate climates over much longer timescales, up to 13 million years, as demonstrated by Howard et al. (1996).

Another scenario is that the grains represent detrital material from earlier sedimentary cycles, with dissolution/precipitation occurring under subaerial conditions. As we do not observe many grains with low relief, V-shaped percussion cracks and dulled surface, prolonged water abrasion was not a significant factor influencing the grains' relief, and it may support the turbiditic flows as the primary depositional agent.

Our observations of physical weathering (Figs 7B, 7C and 7K), which superimposes intense chemical weathering but occurred before glacial transport, closely resemble the micrographs presented by Brown (1973) and Higgs (1979) of freshly weathered quartz from granitic rocks. The separation of the grains from the host rock could explain not only the relative abundance of large conchoidal fractures creating flat cleavage surfaces but also their characteristic appearance. They are usually poorly developed, but occasionally they exhibit highly diversified relief with many linear and arc-shaped steps. Flat cleavage surfaces were associated with glacial or aeolian environments by Vos et al. (2014) and Mahaney (2002), but in our case, we did not observe any microtextures related to aeolian abrasion, and these features were present in every sample, not just those from glacial environments. We also do not observe any fresh microtextures, such as percussion marks or fracture faces, which were reported by Mahaney (2002) and Roverato et al. (2015) from mass-wasted grains. These features are absent in the SEM 1 sample (Sokolica RSF), which was initiated shortly after the LGM. Additionally, a higher frequency of cracks is observed in the SEM 3 and 4 samples, further excluding rock sliding as a mechanism responsible for the decomposition of quartz grains during transport.

A glacial reworking is commonly associated with the occurrence of high-stress microtextures, such as arc-shaped steps, subparallel linear fractures and large conchoidal fractures (Woronko 2016 and references therein). These microtextures we observe in moraine SEM 2 and 3 samples, as well as in the SEM 4 sample, which represents *in situ* weathered slope cover. Thus, we cannot presume that the occurrence of single microtextures is a definitive indicator of a glacial environment. Instead, we attribute mechanically induced microtextures also to P-type frost weathering, which is associated with the movement of quartz grains relative to each other during the growth of ice lenses (Woronko, Hoch 2011, Woronko 2016). Interestingly, the best examples of frost action were found in the SEM 4 sample, where a few grains deviate from the general pattern of frost-weathering microtextures exhibiting poorly developed microrelief (cf. Woronko, Pisarska-Jamroży 2016, Woronko 2016). However, compared with non-glacial SEM 1 and 4 samples, only moraine samples (SEM 2 and 3) show fresh and sharp conchoidal fractures, along with many irregularly spaced subparallel linear fractures and arc-shaped steps, covering at least 50–70% of the grains' surface (Figs 7D, 7E, 7G and 7H). These observations follow Molén's (2014, 2023) conclusions that glaciogenic grains typically exhibit fresh, irregularly abraded surfaces, but indicate that the degree of grain surface transformation is also diagnostic. The presence of breakage blocks could either be the result of subglacial erosion (Sharp, Gomez 1986, Rose, Hart 2008, Woronko 2016), and in the case of SEM 3 sample, a higher proportion of this microtexture also indicates active subglacial transport. Nonetheless, only irregular patterns and large fractures covering most of the grains' surface appear to be the sole distinguishing features between glacially crushed grains and frost-weathered grains, though both processes could have occurred simultaneously under the glacier (Woronko 2016). Using this criterion, in our case, only 5% of the grains were subjected to active subglacial transport during the LGM, and an additional 20% of the grains show a similar appearance, but they are clearly not fresh (Fig. 7F).

The presence of abrasion microtextures, and the general outline of the grains, with large (100–200 μm) conchoidal fractures, indicate effective subglacial crushing and abrasion (Sharp, Gomez 1986, Rose, Hart 2008, Woronko 2016). Recent studies have highlighted that even small mountain glaciers can effectively erode their beds and overprint quartz grains (Engel et al. 2010, 2011, Mentlík et al. 2010, Mahaney et al. 2011, Traczyk, Woronko 2010). Thus, the relatively low percentage of glacial grains in the SEM 2 and 3 samples can be attributed to the mixing of supraglacial material with subglacial till within the moraines, rather than insufficient glacier erosion. It may also explain the occurrence of grains with more weathered (older) abrasion microtextures, which could be the remnants of former glacial advances (pre-LGM) or the effects of frost-derived disintegration. Moreover, the comminution of quartz grains was more intense in the inter-terminal zone than in the accumulation area, which is revealed by the differences in moraine samples – the SEM 3 sample, for example, displays more microtextures such as straight grooves and sawtooth fractures than the SEM 2 sample. There is also a gradual decrease in the obliteration of euhedral quartz, from 85% in SEM 4 (slope covers), to 55% in SEM 2 (cirque moraine), and to 25% in SEM 3 (terminal moraine) which further proves downslope grading glacial reworking.

## Conclusions

In this study, we integrate recently published and new acquired geomorphological data, including mapped glacial landforms, glacier reconstructions and sedimentological documentation, all of which support the presence of local glaciation in the Babia Góra massif. We documented the morphometry of glacial erosional and accumulation features in the Szumiąca Valley, where a small cirque-valley glacier (0.87 km² in area and 2.2 km long) developed during the Late Pleistocene.

The Babia Góra massif is the only region in the Western Carpathians, composed of flysch that was glaciated, where glacial landforms have been significantly (68%) overprinted by subsequent RSF. However, remnants of terminal moraines and a glacial cirque are still preserved in the landscape. We argue that the geomorphological criteria used in previous studies alone are insufficient to confirm or reject glaciation in areas heavily reshaped by landslides. Our findings suggest that the application of clast morphology, quartz grain microtextures and Schmidt-hammer dating overcomes the limitations of traditional geomorphological methods and provides valuable indicators of glacial sediment genesis.

Textural indicators of glacial origin in the sediments are associated with the presence of perched boulders (up to ~3 m in size), a higher proportion of blade- and elongate-shaped forms and more pronounced rounding compared with clasts found in scree and landslide deposits. Glacial reworking of the Magura-type sandstones reduced their initial angularity with only minor shape changes. This is similar to other flysch massifs in the Eastern Carpathians and aligns with the debris cascade model for glaciated areas composed of highly anisotropic rocks (Lukas et al. 2013).

Microscopic analyses revealed that all four samples were primarily composed of chemically altered grains with medium to high relief. Examination of 80 quartz grains from different depositional environments showed that active glacial reworking was the primary process influencing the grains' micromorphology during transport. Although only 5% of the grains could be unambiguously identified as glacially abraded and crushed, due to fresh and irregular fractures on their surfaces, SEM analysis proved useful in distinguishing between glacial and non-glacial samples.

The reconstructed climatic ELA in the study area (1354 m a.s.l.) closely matches the mean elevation of the cirque floor (1357 m), supporting the position of the lowest Pleistocene snow line in the Western Carpathians. The glaciation magnitude is typical of intermediate-level glaciation found in the Svydovets massif, the Pietros group of the Chornohora Mountains and the Maramure-Mountains in the Eastern Carpathian

**Acknowledgements**

We would like to thank the authorities of the Babia Góra National Parks (BPN) for enabling research in the protected area. Special thanks to two anonymous reviewers for their careful reviews and valuable comments that improved the manuscript.

## Authors' contribution

PK: writing – review & editing, writing – original draft, methodology, investigation, formal analysis, conceptualization; DS: SEM analysis, interpretation and writing.

## References


Alexandrowicz S.W., 1978. The northern slope of Babia Góra Mt. as a huge rock slump. *Studia Geomorphologica Carpatho-Balcanica* 12: 133–148.

Ananev G.S. (red.), 1981. *Geomorfologiya osevoj zony Vostochnykh Karpat*. Izd. Moskovskogo Universiteta, Moskva.

Anderson R.S., Duhnforth M., Colgan W., Anderson L., 2012. Far-flung moraines: Exploring the feedback of glacial erosion on the evolution of glacier length. *Geomorphology* 179: 269–285. DOI 10.1016/j.geomorph.2012.08.018

Barr I.D., Lovell H., 2014. A review of topographic controls on moraine distribution. *Geomorphology* 226: 44-64. DOI 10.1016/j.geomorph.2014.07.030.

Barr I.D., Spagnolo M., 2015. Glacial cirques as palaeoenvironmental indicators: Their potential and limitations. *Earth-Science Reviews* 151: 48–78. DOI 10.1016/j.earscirev.2015.10.004.

Benn D.I., Ballantyne C.K., 1994. Reconstructing the transport history of glacigenic sediments: A new approach based on the co-variance of clast form indices. *Sedimentary Geology* 91: 215–227. DOI 10.1016/0037-0738(94)90130-9.

Benn D.I., Ballantyne C.K., 2005. Palaeoclimatic reconstruction from Loch Lomond Readvance glaciers in the West Drumochter Hills, Scotland. *Journal of Quaternary Science* 20(6): 577–592. DOI 10.1002/jqs.925.

Benn D.I., Hulton N.R.J., 2010. An ExcelTM spreadsheet program for reconstructing the surface profile of former mountain glaciers and ice caps. *Computer and Geosciences* 36: 605–610. DOI 10.1016/j.cageo.2009.09.016.

Benn D.I., Lehmkuhl F., 2000. Mass balance and equilibrium-line altitudes of glaciers in high-mountain environments. *Quaternary International* 65–66: 15–29. DOI 10.1016/S1040-6182(99)00034-8.

Brook M.S., Lukas S., 2012. A revised approach to discriminating sediment transport histories in glacigenic sediments in a temperate alpine environment: A case study from Fox Glacier, New Zealand. *Earth Surface Processes and Landforms* 37(8): 895–900. DOI 10.1002/esp.3250.

Brown J.E., 1973. Depositional histories of sand grains from surface textures. *Nature* 242(5397): 396–398. DOI 10.1038/242396a0.

Cailleux A., 1942. Les Actions Eoliens Periglaciaries en Europe. *Memoirs* vol. 21. *Société Géol.*, France, No. 46: 1–176.

Coleman C.G., Carr S.J., Parker A.G., 2009. Modelling topoclimatic controls on palaeoglaciers: Implications for inferring palaeoclimate from geomorphic evidence. *Quaternary Science Reviews* 28: 249–259. DOI 10.1016/j.quascirev.2008.10.016.

Dahl S.O., Nesje A., 1992. Equilibrium-line altitude depressions of reconstructed Younger Dryas and Holocene glaciers in Fosdalen, inner Nordfjord, western Norway. *Norsk Geologisk Tidsskrift* 72: 206–216.

Dobiński W., Glazer M., Bieta B., Mendecki M.J., 2016. Poszukiwanie wieloletniej zmarzliny i budowa geologiczna Babiej Góry w świetle wyników obrazowania elektrooporowego. *Przegląd Geograficzny* 88(1): 31–51. DOI 10.7163/PrzG.2016.1.2.

Doornkamp J.C., Krinsley D., 1971. Electron microscopy applied to quartz grains from a tropical environment. *Sedimentology* 17(1–2): 89–101. DOI 10.1111/j.1365-3091.1971.tb01133.x.

Engel Z., Nývlt D., Křížek M., Treml V., Jankovská V., Lisá L., 2010. Sedimentary evidence of landscape and climate history since the end of MIS 3 in the Krkonoše Mountains, Czech Republic. *Quaternary Science Reviews* 29 (7–8): 913–927. DOI 10.1016/j.quascirev.2009.12.008.

Engel Z., Traczyk A., Braucher R., Woronko B., Křížek M., 2011. Use of 10Be exposure ages and Schmidt hammer data for correlation of moraines in the Krkonoše Mountains, Poland/Czech Republic. *Zeitschrift für Geomorphologie* 55(2): 175–196. DOI 10.1127/0372-8854/2011/0055-0036.

Evans I.S., 1977. World-wide variations in the direction and concentration of cirque and glacier aspects. *Geografiska Annaler Series B* 59(3–4): 151–175. DOI 10.1080/04353676.1977.11879949.

Evans I.S., 2006. Allometric development of glacial cirque form: Geological, relief and regional effects on the cirques of Wales. *Geomorphology* 80: 245–266. DOI 10.1016/j.geomorph.2006.02.013.

Evans I.S., 2021. Glaciers, rock avalanches and the 'buzzsaw' in cirque development: Why mountain cirques are of mainly glacial origin. *Earth Surface Processes and Landforms* 46(1): 24–46. DOI 10.1002/esp.4810.

Fick S.E., Hijmans R.J., 2017. WorldClim 2: New 1 km spatial resolution climate surfaces for global land areas. *International Journal of Climatology* 37(12): 4302–4315. DOI 10.1002/joc.5086.

Glasser N.F., Harrison S., Jansson K.N., 2009. Topographic controls on glacier sediment – Landform associations around the temperate North Patagonian Icefield. *Quaternary Science Reviews* 28(25): 2817–2832. DOI 10.1016/j.geomorph.2019.03.00.

Graham D.J., Midgley N.G., 2000. Graphical representation of particle shape using triangular diagrams: An Excel spreadsheet method. *Earth Surface Processes and Landforms* 25(13): 1473–1477. DOI 10.1002/1096-9837(200012)25:13<1473::AID-ESP158>3.0.CO;2-C.

GUGiK [Główny Urząd Geodezji i Kartografii], 2025 Geoportal. Online: www.geoportal.gov.pl (accessed January 1, 2025).

Hanslik E., 1907. Die Eiszeit in den Schlesischen Beskiden. *Mitteilungen der Österreichischen Geographischen Gesellschaft* 50: 20–32.

Hedding D.W., Sumner P.D., 2013. Diagnostic criteria for pronival ramparts: Site, morphological and sedimentological characteristics. *Geografiska Annaler: Series A, Physical Geography* 95: 315–322. DOI 10.1111/geoa.12021.

Higgs R., 1979. Quartz-grain surface features of Mesozoic-Cenozoic sands from the Labrador and western Greenland continental margins. *Journal of Sedimentary Research* 49(2): 599–610.

Howard J.L., Amos D.F., Daniels W.L., 1996. Micromorphology and dissolution of quartz sand in some exceptionally ancient soils. *Sedimentary Geology* 105(1–2): 51–62. DOI 10.1016/0037-0738(95)00133-6.

Hughes P.D., Gibbard P.L., Woodward J.C., 2007. Geological controls on Pleistocene glaciation and cirque form in Greece. *Geomorphology* 88: 242–253. DOI 10.1016/j.geomorph.2006.11.008.

Jahn A., 1958. Mikrorelief peryglacjalny Tatr i Babiej Góry. *Biuletyn Peryglacjalny* 6: 57–80.

Jankowski L., Garecka M., 2022. *Objaśnienia do Szczegółowej Mapy Polski*. PIG-PIB, Warszawa, Ark. (1031) Zawoja.

Kalińska-Nartiša E., Woronko B., Ning W., 2017. Microtextural inheritance on quartz sand grains from Pleistocene periglacial environments of the Mazovian Lowland, central Poland. *Permafrost and Periglacial Processes* 28(4): 741–756. DOI 10.1002/ppp.1943.

Klimaszewski M. 1952. Zagadnienia plejstocenu południowej Polski. *Biuletyn Państwowego Instytutu Geologicznego* 65: 137–268.

Kłapyta P., 2020. Geomorphology of the high-elevated flysch range – Mt. Babia Góra massif (Western Carpathians). *Journal of Maps* 16: 689–701. DOI 10.1080/17445647.2020.1800530.

Kłapyta P., Bryndza M., Zasadni J., Jasionek M., 2022b. The lowest elevation Pleistocene glaciers in the Carpathians – The geomorphological and sedimentological record of glaciation in the Polonyna Rivna and Borzhava massifs (Ukraine Carpathians). *Geomorphology* 398: 108060. DOI 10.1016/j.geomorph.2021.108060.

Kłapyta P., Mîndrescu M., Zasadni J., 2021a. Geomorphological record and equilibrium line altitude of glaciers during the last glacial maximum in the Rodna Mountains (Eastern Carpathians). *Quaternary Research* 100: 1–20. DOI 10.1017/qua.2020.90.

Kłapyta P., Mîndrescu M., Zasadni J., 2022a. The impact of local topoclimatic factors on marginal Pleistocene glaciation in the Northern Romanian Carpathians. *Catena* 210: 105873. DOI 10.1016/j.catena.2021.105873.

Kłapyta P., Mîndrescu M., Zasadni J., 2023b. Late Pleistocene glaciation in the headwaters of the Ceremuşul Alb valley (Maramureş Mountains, Romania). *Geographica Polonica* 96: 13–28. DOI 10.7163/GPol.0243.

Kłapyta P., Zasadni J., 2018. Research history on the Tatra Mountains glaciations. *Studia Geomorphologica Carpatho-Balcanica* 51–52: 43–85.

Kłapyta P., Zasadni J., Dubis L., Świąder A., 2021b. Glaciation in the highest parts of the Ukrainian Carpathians (Chornohora and Svydovets massifs) during the local last glacial maximum. *Catena* 203: 105346. DOI 10.1016/j.catena.2021.105346.

Kłapyta P., Zasadni J., Mîndrescu M., 2023a. Late Pleistocene glaciation in the Eastern Carpathians – A regional overview. *Catena* 224: 1-20. DOI 10.1016/j.catena.2023.106994.

Kłapyta P., Zasadni J., Mîndrescu M.,Dubis L., 2024. Glacial geomorphology and glacier reconstruction in the Maramureş Mountains (Romania and Ukraine). *Geoconcept* 1:80-102.

Kłapyta P., Zatorski M., Kondracka M., 2025. Evolution of rock slope failures in the flysch area – Insight from the Babia Góra massif (Western Carpathians, Poland). *Catena* 254: 1-17.108948. DOI 10.1016/j.catena.2025.108948.

Klimaszewski M., 1948. *Polskie Karpaty Zachodnie w okresie dyluwialnym*. Prace Wrocławskiego Towarzystwa Naukowego, Wrocław: 7.

Krumbein W.C., 1941. Measurement and geological significance of shape and roundness of sedimentary particles. *Journal of Sedimentary Research* 11(2): 64–72. DOI 10.1306/D42690F3-2B26-11D7-8648000102C1865D.

Książkiewicz M., 1963. Zarys geologii Babiej Góry. *Zakład Ochrony Przyrody PAN* 22: 69–87.

Książkiewicz M., 1966. Geologia regionu babiogórskiego. *Przewodnik XXXIX Zajadu Polskiego Towarzystwa Geologicznego* 5–59.

Książkiewicz M., 1971. *Szczegółowa mapa geologiczna Polski 1:50 000, arkusz Zawoja*. Instytut Geologiczny.

Książkiewicz M., 1983. The geology of the Babia Góra region. In: K. Zabierowski (Ed.), National Park on the Babia Góra Mt. Nature and Man. *Studia Naturae B* 29: 25–39.

Łajczak A., 1981. Formy glacjalne na Babiej Górze. *Prace Babiogórskie* 3: 43–53.

Łajczak A., 1998. *Distribution of glacial and nival forms in the Babia Góra massif, Western Carpathians*. Proceedings of the 4th Meeting of Polish Geomorphologists Part II, Lublin: 349–356.

Łajczak A., 2013. Relief development of a highly elevated monoclinal Babia Góra range built by Magura sandstone, Western Carpathian Mts. In: Migoń P., Kasprzak M. (eds), *Sandstone landscapes. Diversity, ecology and conservation*. Eds. Edn. Proc. of Wrocław University: 100–105.

Łajczak A., 2015. *Monografia masywu Pilska (Beskid Żywiecki)*. Instytut Botaniki im. W. Szafera Polskiej Akademii Nauk, Kraków.

Łajczak A., 2016. Wody Babiej Góry. In: *Monografie Babiogórskie. Babiogórski Park Narodowy*. Homago Studio Graficzne, Maków Podhalański.

Łajczak A., 2023. Mt. Babia Góra—The highest flysch ridge in the western Carpathians. In: Migoń P., Jancewicz K. (eds), *Landscapes and landforms of Poland*. Springer: 249–268. DOI 10.1007/978-3-031-45762-3_13.

Łajczak A., Margielewski W., Zielonka T., Pasierbek T., Lamorski T., Kozina P., Izworska K., 2023. Cylowa Zerwa landslide – Debris flow forms on Mount Babia Góra (1725) and their development over the last ca. 150 years, Western Carpathians. *Geographia Polonica* 96(1): 79–101. DOI 10.7163/GPol.0247.

Łajczak A., Migoń P., 2007. The 2002 debris flow in the Babia Góra massif – Implications for the interpretation of mountainous Geomorphic systems. *Studia Geomorphologica Carpatho-Balcanica* 51: 97–116.

Łajczak A., Włoch E., 2004. Gołoborza na Babiej Górze i ich znaczenie paleogeograficzne. In: Łajczak A. (ed.), *Pokrywy stokowe gór średnich strefy umiarkowanej i ich znaczenie paleogeograficzne*. Warsztaty Geomorfologiczne, Zawoja.

Lukas S., Benn D.I., Boston C.M., Brook M., Coray S., Evans D.J.A., Graf A., Kellerer- Pirklbauer A., Kirkbride M.P., Krabbendam M., Lovell H., Machiedo M., Mills S.C., Nye K., Reinardy B.T.I., Ross F.H., Signer M., 2013. Clast shape analysis and clast transport paths in glacial environments: A critical review of methods and the role of lithology. *Earth-Science Reviews* 121: 96–116. DOI 10.1016/j.earscirev.2013.02.005.

Lukniš M., 1964. The course of the last glaciation of the Western Carpathians in the relation to the Alps, to the glaciation of northern Europe, and to the division of the central European Würm into periods. *Geograficky Časopis, SAV* 16(2): 127–142. (in Slovak).

Maglay J., Moravcová M., Šefčík P., Vlačíki M., Pristaš J., 2011. *Prehľadná geologická mapa kvartéru Slovenska, 1: 200 000*. Štatny geologicky ustav Dionyza Štura, Bratislava.

Mahaney W.C., 2002. Atlas of sand grain surface textures and applications. Oxford University Press.

Mahaney W.C., Hancock R.G., Melville H., 2011. Late glacial retreat and Neoglacial advance sequences in the Ziller-

tal Alps, Austria. *Geomorphology* 130(3–4): 312–326. DOI 10.1016/j.geomorph.2011.04.013.

Mentlík P., Minár J., Břízová E., Lisá L., Tábořík P., Stacke V., 2010. Glaciation in the surroundings of Prášilské Lake (Bohemian Forest, Czech Republic). *Geomorphology* 117(1–2): 181–194. DOI /10.1016/j.geomorph.2009.12.001.

Midowicz W., 1974. Babia Góra. Monografia turystyczna. *Karpaty* 2: 61–96.

Miller H.P., 1963. *Struktura, genezis i voprosy racionalnogo ispolzovaniya landshafta Chernogory v Ukrainskikh Karpatakh*: avtoref. dis. na soisk. uch. stupeni kand. geogr. nauk: spec. 11.00.01. Lvov.

Mîndrescu M., Evans I.S., 2014. Cirque form and development in Romania: Allometry and the buzzsaw hypothesis. *Geomorphology* 208: 117–136. DOI 10.1016/j.geomorph.2013.11.019.

Mitchell W.A., 1996. Significance of snowblow in the generation of Loch Lomond Stadial (Younger Dryas) glaciers in the western Pennines, northern England. *Journal Of Quaternary Science* 11: 233–248. DOI 10.1002/(SICI)1099-1417(199605/06)11:3<233::AID-JQS240>3.0.CO;2-Q.

Molén M.O., 2014. A simple method to classify diamicts by scanning electron microscope from surface microtextures. *Sedimentology* 61(7): 2020–2041. DOI 10.1111/sed.12127.

Molén M.O., 2023. Patterns, processes and models – An analytical review of current ambiguous interpretations of the evidence for pre-Pleistocene glaciations. *Geologos* 29(3): 139–166. DOI 10.14746/logos.2023.29.3.15.

Mycielska-Dowgiałło E., Woronko B., 1998. Analiza obtoczenia i zmatowienia ziarn kwarcowych frakcji piaszczystej i jej wartość interpretacyjna. *Przegląd Geologiczny* 46(12): 1275–1281.

Niedźwiedź T., Orlicz M., Orliczowa J., 1985. Wiatr w Karpatach Polskich. In: *Dokumentacja Geograficzna*. IG i GP PAN: 6.

Niemirowski M., 1963. Szkic geograficzny obszaru babiogórskiego. *Zakład Ochrony Przyrody PAN* 22: 21–43.

Obrębska-Starklowa B., 2004. Klimat masywu Babiej Góry. In: Wołoszyn B.W., Jaworski A., Szwagrzyk J. (eds), *Babiogórski Park Narodowy – monografia przyrodnicza*. Komitet Ochrony Przyrody PAN, Babiogórski Park Narodowy: 137–151.

Oien R.P., Spagnolo M., Rea B.R., Barr I.D., Bingham R.G., 2020. Climatic controls on the equilibrium-line altitudes of Scandinavian cirque glaciers. *Geomorphology* 352: 1–11. DOI 10.1016/j.geomorph.2019.106986.

Paulo K., 1937. Zjawiska glacjalne i periglacjalne w Małej Fatrze. *Badania Geograficzne* 18-19: 71–115.

Pawłowski S., 1933. Z badan nad zlodowaceniem polskich Karpat. *Czasopismo Geograficzne* 11(1–2): 1–5.

Pawłowski S., 1936. Les Karpates a l'epoque glaciaire. Congres Internationale de Geographie (Varsovie 1934). *Comptes Rendus, Travaux de section* 2: 89–141.

Pax F., 1905. Vegetation der Babiagura. *Mitteilungen des Beskidenvereines* 2(1): 5.

Pedersen V.K., Egholm D.L., 2013. Glaciations in response to climate variations preconditioned by evolving topography. *Nature* 493(7431): 206–210. DOI 10.1038/nature11786.

Pellitero R., Rea B.R., Spagnolo M., Bakke J., Hughes P., Ivy-Ochs S., Lukas S., Ribolini A., 2015. A GIS tool for automatic calculation of glacier equilibrium-line altitudes. *Computers and Geosciences* 82: 55–62. DOI 10.1016/j.cageo.2015.05.005.

Powers M.C., 1953. A new roundness scale for sedimentary particles. *Journal of Sedimentary Research* 23(2): 117–119. DOI 10.1306/D4269567-2B26-11D7-8648000102C1865D.

Pye K., 1983. Formation of quartz silt during humid tropical weathering of dune sands. *Sedimentary Geology* 34(4): 267–282. DOI 10.1016/0037-0738(83)90050-7.

Pye K., Mazzullo J., 1994. Effects of tropical weathering on quartz grain shape; an example from northeastern Australia. *Journal of Sedimentary Research* 64(3a): 500–507. DOI 10.1306/D4267DE8-2B26-11D7-8648000102C1865D.

Pyrda A., 2025. *Zlodowacenie północnego skłonu Tatr Niżnych.* MS, Uniwersytet Komisji Edukacji Narodowej w Krakowie, Kraków.

Rose K.C., Hart J.K., 2008. Subglacial comminution in the deforming bed: Inferences from SEM analysis. *Sedimentary Geology* 203(1–2): 87–97. DOI 10.1016/j.sedgeo.2007.11.003.

Roverato M., Cronin S., Procter J., Capra L., 2015. Textural features as indicators of debris avalanche transport and emplacement, Taranaki volcano. *Geological Society of America Bulletin* 127(1–2): 3–18. DOI 10.1130/B30946.1.

Ruszkiczay-Rüdiger Z., Kern Z., Urdea P., Madarász B., Braucher R., ASTER Team., 2021. There was limited glacial erosion during the last glaciation in mid-latitude cirques (Retezat Mts, Southern Carpathians, Romania). *Geomorphology* 384: 107719. DOI 10.1016/j.geomorph.2021.107719.

Ruszkiczay-Rüdiger Z., Temovski M., Kern Z., Madarász B., Milevski I., Lachner J., Steier P., 2022. Late Pleistocene glacial advances, equilibrium-line altitude changes and paleoclimate in the Jakupica Mts (North Macedonia). *Catena* 216: 106383. DOI 10.1016/j.catena.2022.106383.

Sawicki L., 1912. Les ´etudes glaciaire dans les Karpates. Aperçu historique et critique. Annales de G´eographie, Paris: 21.

Sawicki L., 1913. Krajobrazy lodowcowe Zachodniego Beskidu. *Rozprawy Wydziału Matematyczno-Przyrodniczego PAU* 53: 1–21.

Schulz M.S., White A.F., 1999. Chemical weathering in a tropical watershed, Luquillo Mountains, Puerto Rico III: quartz dissolution rates. *Geochimica et Cosmochimica Acta* 63(3–4): 337–350. DOI 10.1016/S0016-7037(99)00056-3.

Sharp M., Gomez B., 1986. Processes of debris comminution in the glacial environment and implications for quarts sand-grain micromorphology. *Sedimentary Geology* 46(1–2): 33–47. DOI 10.1016/0037-0738(86)90004-7.

Sikora W., Żytko K., 1960. Budowa Beskidu Wysokiego na południe od Żywca (Geology of the Beskid Wysoki range south of Żywiec, Western Carpathians). *Biuletyn Instytutu Geologicznego* 141: 61–204.

Sîrcu I., 1962. Rolul alunecarilor şi prabuşirilor de mase de roci în formarea reliefului munţilor cristalini ai Rodnei, Anal. şt. Univ. « Al. I. Cuza » Iaşi, (Seria noua), secţ. II (Şt. nat), b. *Geologie- Geografie* 8: 81–94.

Sîrcu I., 1963. Le probleme de la glaciation quaternaire dans les montagnes du Maramureş, Anal. şt. Univ. `Al. I. Cuza` Iaşi, (Seria noua), secţ. II (Şt. nat), b. *Geologie- Geografie* 9: 125–134.

Sissons J.B., Sutherland D.G., 1976. Climatic inferences from glaciers in the South-East Grampian Highlands, Scotland. *Journal of Glaciology* 17: 325–346. DOI 10.3189/S0022143000013617.

Sneed E.D., Folk R.L., 1958. Pebbles in the lower Colorado River, Texas, a study in particle morphogenesis. *Journal of Geology* 66: 114–150.

Spagnolo M., Pellitero R., Barr I.D., Ely J.C., Pellicer X.M., Rea B.R., 2017. ACME, a GIS tool for automated cirque metric extraction. *Geomorphology* 278: 280–286. DOI 10.1016/j.geomorph.2016.11.018.

Starkel L., 1960. Rozwój rzeźby Karpat fliszowych w holocenie. *Prace Geograficzne IG PAN* 22.

Świderski B., 1938. *Geomorfologia Czarnohory*. Wyd. Kasy im, Mianowskiego, Warszawa.

Tietze E., 1888. *Geologische Beschreibung des Gebieten von Krakau*. Jahrbuch dar k. k. Geol, Reichsanstalt. Wien.

Traczyk A., Woronko B., 2010. Historia zlodowacenia doliny Łomnicy w Karkonoszach w zapisie mikromorfologii powierzchni ziarn kwarcu. *Przegląd Geologiczny* 58(12): 1182–1191.

Urdea P., Ardelean F., Ardelean M., Onaca A., Hughes P.D., 2022. Glacial landscapes of the Romanian Carpathians. 109–114. DOI 10.1016/B978-0-12-823498-3.00031-5

Vos K., Vandenberghe N., Elsen J., 2014. Surface textural analysis of quartz grains by scanning electron microscopy (SEM): From sample preparation to environmental interpretation. *Earth-Science Reviews* 128: 93–104. DOI 10.1016/j.earscirev.2013.10.013.

Whalley W.B., 2009. On the interpretation of discrete debris accumulations associated with glaciers with special reference to the British Isles. In: Knight, J., Harrison, S. (Eds.), Periglacial and Paraglacial Processes and Environments. *Geological Society London, Special Publications* 320: 85–102. DOI 10.1144/SP320.7.

Wilner J.A., Nordin B.J., Getraer A., Gregoire R.M., Krishna M., Li J., Pickell D.J., Rogers E.R., McDannell K.T., Palucis M.C., Keller C.B., 2024. Limits to timescale dependence in erosion rates: Quantifying glacial and fluvial erosion across timescales. *Science Advances* 10: 51. DOI 10.1126/sciadv.adr2009.

Wójcik A., 1994. Osady glacjalne i osuwiskowe Pilska (Beskid żywiecki). *Biuletyn Państwowego Instytutu Geologicznego* 369: 49–62.

Wójcik A., Rączkowski W., Mrozek T., Nescieruk P., Marciniec P., Zimnal Z., 2010. *Babiogórski Park Narodowy 1: 13 000*. Ministerstwo Środowiska, Warszawa.

Woronko B., 2016. Frost weathering versus glacial grinding in the micromorphology of quartz sand grains: Processes and geological implications. *Sedimentary Geology* 335: 103–119. DOI 10.1016/j.sedgeo.2016.01.021.

Woronko B., Hoch M., 2011. The development of frost-weathering microstructures on sand-sized quartz grains: Examples from Poland and Mongolia. *Permafrost and Periglacial Processes* 22(3): 214–227. DOI 10.1002/ppp.725.

Woronko B., Pisarska-Jamroży M., 2016. Micro-scale frost weathering of sand-sized quartz grains. *Permafrost and Periglacial Processes* 27(1): 109–122. DOI 10.1002/ppp.1855.

Wray R.A., Sauro F., 2017. An updated global review of solutional weathering processes and forms in quartz sandstones and quartzites. *Earth-Science Reviews* 171: 520–557. DOI 10.1016/j.earscirev.2017.06.008.

Zasadni J., Kałuża P., Kłapyta P., Świąder A., 2021. Evolution of the Białka valley Pleistocene moraine complex in the High Tatra Mountains. *Catena* 207: 105704. DOI 10.1016/j.catena.2021.105704.

Zasadni J., Kłapyta P., 2014. The Tatra Mountains during the last glacial maximum. *Journal of Maps* 1264(10): 440–456. DOI 10.1080/17445647.2014.885854.

Zasadni J., Kłapyta P., Broś E., Ivy-Ochs S., Świąder A., Christl M., Balážovičová L., 2020. Latest Pleistocene glacier advances and post-Younger Dryas rock glacier stabilization in the Mt. Kriváň group, High Tatra Mountains, Slovakia. *Geomorphology* 358: 107093. DOI 10.1016/j.geomorph.2020.107093.

Zasadni J., Kłapyta P., Kałuża P., Makos M., 2022. The Tatra Mountains: Glacial landforms prior to the last glacial maximum. In: Palacios D., Hughes P.D., García-Ruiz J.M., de Andrés N. (red.) (eds), *European glacial landscapes: Maximum extent of glaciations*. Elsevier, Amsterdam, Oxford, Cambridge: 271–275. DOI 10.1016/B978-0-12-823498-3.00059-5.

Zasadni J., Kłapyta P., Świąder A., 2018. Predominant western moisture transport to the Tatra Mountains during the last glacial maximum, inferred from glacier palaeo-ELAs. *XXI International Congress of the CBGA*.

Žebre M., Stepišnik U., 2014. Reconstruction of Late Pleistocene glaciers on Mount Lovcen. *Quaternary International* 353: 225–235.

Ziętara T., 1962. O pseudoglacjalnej rzeźbie Beskidów Zachodnich. Rocznik Naukowo-Dydaktyczny WSP. *Geografia* 10: 69–87.

Ziętara T., 1989. Rozwój teras krioplanacyjnych w obrębie wierzchowiny Babiej Góry w Beskidzie Wysokim. *Folia Geographica*, ser. *Geographia Physica* 21: 79–92.

Ziętara K., Ziętara T., 1958. O rzekomo glacjalnej rzeźbie Babiej Góry. Rocznik Naukowo-Dydaktyczny WSP. *Geografia* 8: 55–78.